Review

Single-Atom Nanomaterials in Electrochemical Sensors Applications

Jinglin Fu and **Yang Liu** *

Department of Chemistry, Beijing Key Laboratory for Analytical Methods and Instrumentation, Kay Lab of Bioorganic Phosphorus Chemistry and Chemical Biology of Ministry of Education, Tsinghua University, Beijing 100084, China
* Correspondence: liu-yang@mail.tsinghua.edu.cn; Tel.: +86-10-62798187

Abstract: In recent years, the development of highly sensitive sensors has become a popular research topic. Some functional nanomaterials occupy an important position in the sensing field by virtue of their unique structures and catalytic properties, but there are still problems such as low sensitivity and poor specificity. Single-atom nanomaterials (SANs) show significant advantages in amplifying sensing signals and improving sensor interference resistance due to their high atomic utilization, structural simplicity, and homogeneity. They are expected to achieve high sensitivity and high specificity monitoring by modulating the active sites. In this review, the recent progress on SANs for electrochemical sensing applications was summarized. We first briefly summarize the features and advantages of single-atom catalysts. Then recent advances in the regulation of reaction sites in noble and non-noble metal-based SANs, including the introduction of defects in the carrier, other metal atoms, and ligand atoms, were highlighted. After that, the SANs for the construction of electrochemical, electrochemiluminescent (ECL), and photoelectrochemical (PEC) sensors and their applications in biochemical and environmental analysis were demonstrated. Finally, the future research aspect of SANs-based electrochemical sensing and the challenges of the SANs design and structure-properties revelation were illustrated, giving guidance on sensitive and accurate biosensing toward clinic diagnostic and environmental analysis.

Keywords: single-atom nanomaterial; electrochemical; sensor

1. Introduction

Electrochemical analysis is a technique that involves the measurement of electrical signals from chemical reactions occurring at the electrode interface [1]. Because of the obvious advantages of high sensitivity, fast response time, simple operation, and miniaturization, electrochemical sensors have become an important analytical tool in areas such as environmental and biological samples [2]. In recent years, as researchers have been studying the physicochemical properties of nanomaterials, it has been possible to achieve precise modulation of their structure and size to a large extent, which has led to many critical breakthroughs in the utilization of nanomaterials as sensing interfaces for signal amplification and interfacial biomolecule recognition [3]. However, the extensive application of electrochemical sensors is still limited by their low sensitivity for the detection of trace substances, and their specificity in complex biological systems is yet to be improved. Since the chemical and physical features of nanomaterials are highly correlative to their intrinsic properties such as surface areas, numbers of active sites, morphologies, etc., precise control of their structures can not only improve catalytic activity and amplify signals but also facilitate specific identification of the analytes to be detected, thus promoting the performance of electrochemical sensors in clinical diagnosis, environmental analysis, and so on [4,5]. In these years, SANs have received much attention since their introduction due to their special geometry and electronic structure, and the precise metal sites of SANs cater to the challenges encountered in the sensitivity and specificity of electrochemical sensors [6].

SANs are distinguished by the isolated metal atoms dispersed on the support material and the absence of metal–metal bonds. SANs not only maximize atomic utilization and have unique electronic structures and atomic coordination environments, but more importantly, the simplicity and homogeneity of their structures facilitate the accurate identification and characterization of active sites, which can provide insight into the structure–activity relationship and make reasonable regulation of them possible [7,8]. These merits enable SANs to be effective materials for the development of sensors with high analytical performance and defined mechanisms. The presence of a large number of unsaturated, low-coordinated metal atoms in SANs facilitates signal amplification and also improves the selectivity of detection by adjusting the metal centers and their coordination environment, which is conducive to achieving sensitive detection of trace substances. By adjusting the structure of SANs, researchers have continuously optimized their sensitivity, selectivity, and stability in sensing, making them great candidates for development in analytical chemistry [1,9,10]. According to the classification of support materials, they broadly include metal–carbon-based materials [11–16], metal–metal oxides [17–19], metal–metal sulfides [20–22], and metal–metal substrates [23,24] (i.e., single-atom alloys) synthesized mainly through three strategies, including defect engineering strategy, spatial confinement strategy, and sacrificial template-assisted strategy (Figure 1).
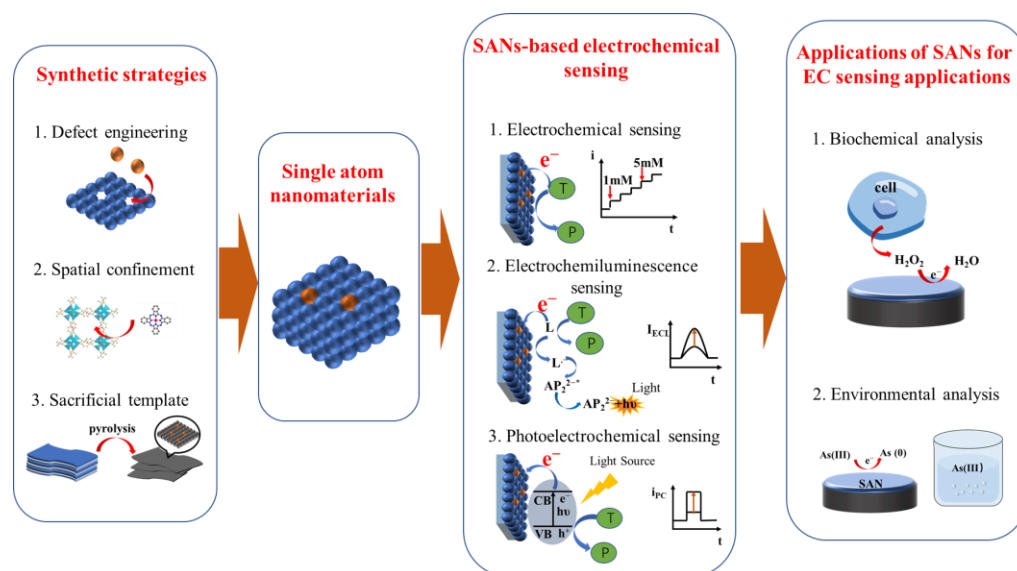

Figure 1. Schematic illustration of the main content of this review.

In this review, we systematically summarize recent advances in SANs for applications in catalytic performance optimization and electrochemical sensing. Firstly, the recent achievements in the modulation of the active sites, including the noble and non-noble metal-based SANs, are presented. The active centers of SANs are mostly the metallic atoms in them, which are not only affected by the metal species but also the numbers of the metal centers as well as their coordinative environment. In this way, the properties of the SANs can be modulated by the central metal atoms and their coordination environment. Then, the research progress of SANs in electrochemistry [25–27], electrochemiluminescence (ECL) [28,29], and photoelectrochemical (PEC) [30,31] sensing for environmental and biochemical sample analysis was highlighted, which has demonstrated large potential for in vivo and in vitro detection of biological samples as well as environmental samples. Finally, the challenges and opportunities for the application of SANs in the field of electrochemical sensing are illustrated (Figure 1).

2. Active Centers Modulation of SANs

The active sites are the catalytically active parts of the SAN, including the metal center and its coordination atoms, which directly affect the catalytic activity and selectivity of the

SAN. The metal centers of the SANs are generally transition metals. Most conventional electrocatalysts are based on noble metals, which have been widely used in catalysis due to their unique intrinsic properties and irreplaceable catalytic activity, such as Pt [18], Pd [32], Ru [33], Rh [34–36], Ir [37], Ag [35,38], Au [39], etc. In order to solve the problems of high cost and low reserves, a series of non-noble metal elements with highly active and economical alternatives have been developed in recent years, such as Fe [40,41], Co [42–44], Cu [45,46], Mn [47], Mo [48], Zn [49], Ni [50,51], etc. The transition metals have empty d or f orbitals and can form coordination bonds with substrate molecules, which facilitates the binding of analytes to SANs [52]. These metals can be dispersed on the supports as single or multiple atoms, and the specific recognition of the analyte can be achieved by modulation of the metal centers. The metal atoms in SANs are isolated and confined within the support materials and are given specific coordination environments. The differences in coordination environments result in distinct electronic structures and densities and thereby can affect the binding energy between substances and SANs as well as the adsorption energy of some reaction intermediates and products, which are important factors in determining catalytic activity and the specificity of sensing. Therefore, methods such as heteroatom doping and axial ligand modulation are also effective ways to modulate the sensing performance of SANs. The following section reviews the work on improving the catalytical activities of noble metal-based and non-noble metal-based SANs by modulating the active centers.

2.1. Noble Metal-Based SANs

Noble metals have been widely studied in the fields of catalysis and sensing due to their superior properties, but high costs and small reserves have severely limited their large-scale applications. The most significant advantage of SANs is the maximization of atomic utilization, which means less waste of active sites and the promise of achieving the same activity with reduced metal loading. Therefore, combining noble metal materials with single-atom strategies is undoubtedly the most effective way to reduce costs. By modifying single Pt atoms on carbon nitride nanorods, SA–Pt/g–C_3N_4–K with peroxidase (POD)-mimicking activity was obtained and used to construct H_2O_2 and antibiotic sensors [53]. After experimental investigation, the enzyme activity of SA–Pt/g–C_3N_4–K was found to be the highest at pH = 4 and 48 °C. Moreover, compared with the natural enzyme horseradish peroxidase (HRP), SA–Pt/g–C_3N_4–K can maintain catalytic stability over a wider temperature range. The POD activities of SA–Pt/g–C_3N_4–K, g–C_3N_4–K, and HRP were compared by colorimetric method using UV-vis absorption spectroscopy with 1 mM tetramethylbenzidine (TMB) and 1 mM H_2O_2 at pH = 4. It was found that SA–Pt/g–C_3N_4–K exhibited higher POD-like activity (Figure 2), which could be targeted to improve the sensitivity of detecting H_2O_2. More than just H_2O_2 sensors, Pt-based SANs can also be utilized for the detection of glucose. A Pt single-atom material on Cu@CuO core-shell nanowires (NWs) has been fabricated by Zhao et al [54]. Cu NWs were first synthesized and further oxidized to Cu@Cu_xO core-shell NWs by oxidation with H_2O_2, and then Pt atoms were anchored to Cu@CuO NWs by an impregnation method and were modified on a glassy carbon electrode (GCE) for glucose sensing. Pt_1/Cu@ CuO NWs can catalyze the oxidation of glucose and exhibit a lower onset potential and higher response current than Cu@CuO and Cu NWs. The introduction of the oxidation layer and single Pt atom improved the electron transfer ability and glucose adsorption ability of the nanomaterials, and this Pt_1/Cu@CuO NWs-based glucose sensor not only had high sensitivity but also good anti-interference ability and long-term stability. Theoretical calculations show that the excellent sensing performance of Pt_1/Cu@CuO NWs stems from the synergistic effect between single Pt atoms and Cu@CuO core-shell NWs, which results in the strong binding energy of glucose on the NWs. Since the doping of other elements (e.g., O, P, S, B, and Cl) in SANs with metal–N–C coordination structures (M–N–C) can modulate the electronic structure of the central metal atom through the electronegativity difference of the heteroatoms, this has become an effective strategy to improve the catalytic activity of SANs. A single-atom nanozyme (SAE) with unique Pt_1–N_3PS active centers has been designed by Chen et al. [55],

and in this work, the direct atomization of Pt nanoparticles (NPs) into single atoms by reversing the thermal sintering process was first reported. This Pt SAN exhibited significant POD-like catalytic activity and kinetics that far surpassed those of Pt NPs. High-angle annular dark field-scanning transmission electron microscopy equipped with a spherical aberration corrector (AC HAADF-STEM) image provided a bright contrast of metal atoms against the low background, in which the atomically dispersed Pt sites could be clearly observed. No Pt–Pt peaks were observed in Fourier-transformed extended Pt L-edge X-ray absorption fine structure (EXAFS) spectra, which suggested that the Pt atoms exist as isolated single-atoms. Pt L_3-edge X-ray absorption near edge structure (XANES) curves indicated that the adsorption threshold of Pt single-atom nanozyme (Pt$_{TS}$-SAzyme) was located between those of PtO_2 and Pt foil, showing that the Pt species carry a positive charge. The EXAFS fitting analysis results revealed that a Pt atom is coordinated to N, S, and P with coordination numbers 2.5, 1, and 1, respectively. The experimental XANES spectrum of Pt$_{TS}$-SAzyme matched well with the calculated XANES spectra, further proving the existence of the Pt_1–N_3SP site (Figure 3A–D). The excellent catalytic performance for oxygen reduction reaction (ORR) of SANs has been investigated for the amplification of electrochemiluminescence (ECL) sensing signals to improve the sensitivity of detection [56]. Therefore, improving the ORR catalytic performance of SANs through ligand environment modulation also has an important role in the sensing field. Qin et al. [57] have reported a Ru-based SAN more durable than the 3D transition metal-based SANs, in which the second coordination shell of Ru centers was doped with S anions bonded to N. S anions in the second coordination shell modulated the energy barrier in the ORR reaction by adjusting the electronic structure of Ru centers, resulting in higher ORR catalytic activity than commercial Pt/C. The Bader charge analysis of RuN_4–S and RuN_4 without S revealed that the S coordination leads to a significant increase in the charge density of the Ru sites, reducing their binding energy to OOH*, O*, and OH*, which results in a higher ORR catalytic activity of Ru–SAN/SNC than Ru–SAN/NC (Figure 4A–D). RuN_4–S (S bonded to the N atom of the second shell layer) and RuN_3S (S bonded directly to the Ru atom of the first shell layer) were also compared, and the evaluation result showed that the binding energy of RuN_4–S is greater than that of Ru–N_3S, thus the RuN_4–S conformation is more easily formed. The introduction of other metal atoms in the active site can also optimize the sensing performance through synergistic effects. Catalysts with atomically dispersed Ru_3 sites were reported by Wu et al. to have higher electrocatalytic activity for uric acid (UA) than Ru SAN [58]. This was due to the optimized electronic structure of the multi-atom sites, which facilitates the adsorption of hydroxyl anion intermediates. Owing to the excellent catalytic activity for the oxidation of small biomolecules of Ru_3/NC, it could be used to construct electrochemical sensors with high sensitivity for UA detection in serum samples, which had broad practical application prospects.
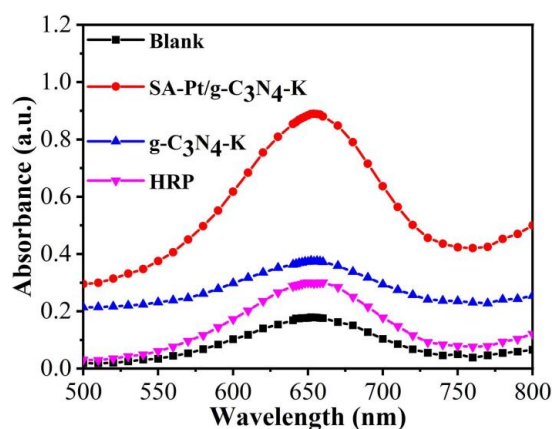

Figure 2. UV–vis absorption spectra of SA–Pt/g–C_3N_4–K, g–C_3N_4–K, and HRP with 1 mM TMB and 1 mM H_2O_2 at pH = 4 [53]. Copyright 2021 with permission from Elsevier.
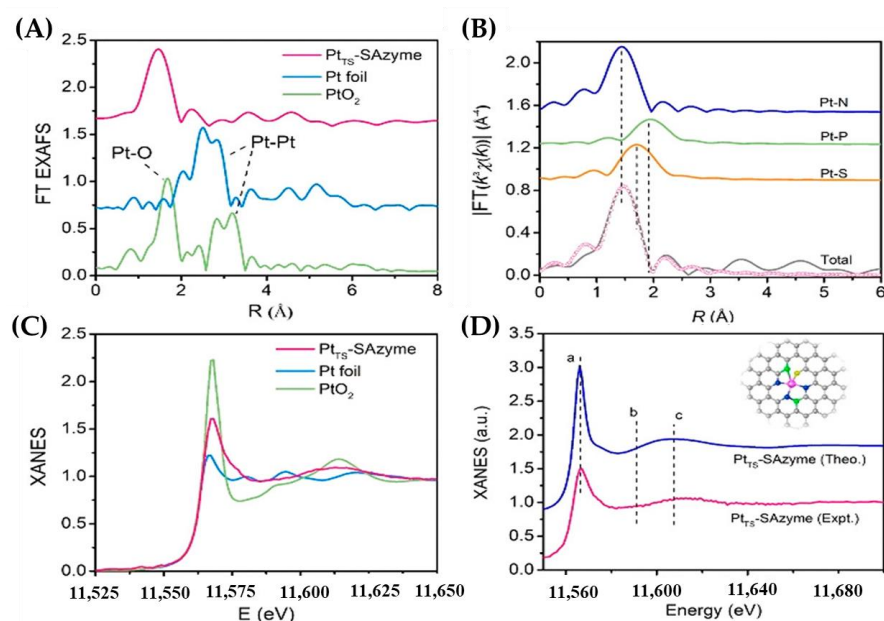
Figure 3. Atomic structural analysis of Pt$_{TS}$-SAzyme. (**A**) Fourier-transformed magnitudes of the experimental Pt L$_3$-edge EXAFS signals of Pt$_{TS}$-SAzyme, Pt foil, and PtO$_2$. (**B**) EXAFS fitting analysis of Pt$_{TS}$-SAzyme in R space. Curves from top to bottom are the Pt–N, Pt–P, and Pt–S three-body backscattering signals, the fitting curve total signal (pink line), and the experimental signal (gray line). (**C**) Pt L$_3$-edge XANES spectra of Pt$_{TS}$-SAzyme, Pt foil, and PtO$_2$. (**D**) Comparison between the experimental XANES spectra (pink line) and the theoretically simulated XANES spectra (blue line) of Pt$_{TS}$-SAzyme (a, b and c indicate the comparison of the shapes of the two spectra.) [55]. Copyright © 2021 American Chemical Society.
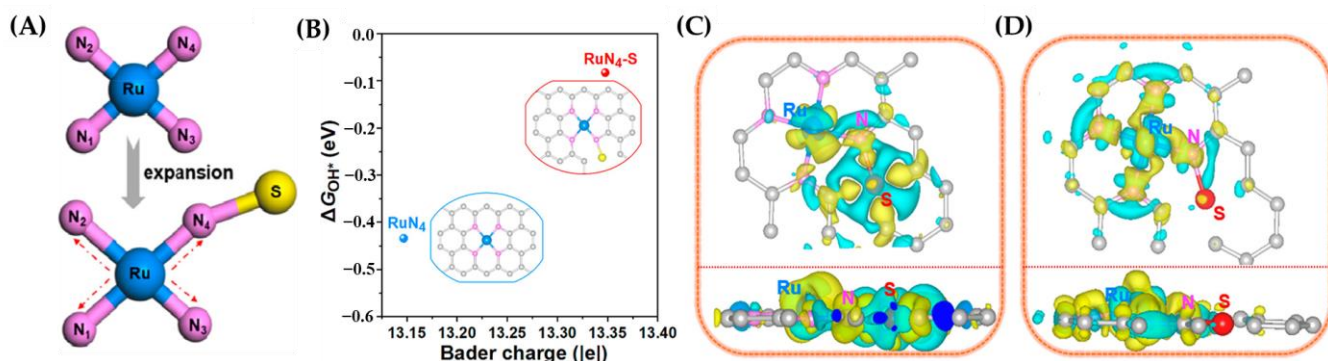

Figure 4. (**A**) Schematic atomic model of Ru–N bond length changes before and after S introduction. Color scheme: blue for Ru, yellow for S, pink for N, and gray for C. (**B**) Relationship between Bader charge and OH* binding energy of single-atom Ru in RuN$_4$ and RuN$_4$–S, respectively. Insert: the corresponding schematic models of the samples. Color scheme: blue for Ru, yellow for S, pink for N, and gray for C. Charge density difference between (**C**) S as the target and (**D**) Ru as the target in the RuN$_4$–S moiety. Color scheme: blue for Ru, red for S, pink for N, and gray for C. Yellow regions indicate charge accumulation, while cyan regions indicate charge depletion [57]. Copyright © 2022 American Chemical Society.

2.2. Non-Noble Metal-Based SANs

The high cost and limited availability of noble metals pose a significant challenge to sustainability. Non-noble metals are now widely used in various fields as cost-effective and sustainable alternatives to other commonly used, expensive transition metals, and their fabrication into single atoms can further amplify the advantages and improve their performance in analysis. As the most widely studied SAN, Fe SANs have demonstrated

excellent catalytic performance and application potential, especially their ORR catalytic ability and enzyme-like activity. A nanozyme with single Fe atoms anchored on N-doped carbon nanotubes (CNT/FeNC) was proposed by Cheng et al. [59], in which the individual iron atoms were all surface atoms and had high structural similarity to the active center in natural PODs, thus possessing the most adequate enzyme-like reaction active centers and better POD-like activity. Its application as a signal element in the construction of a series of paper-based biosensors has successfully achieved the sensitive detection of H_2O_2, glucose, and ascorbic acid (AA), providing a novel and efficient signal element for the construction of future biosensors. The synergy of two non-noble metal atoms has also proven to be an effective way to improve detection sensitivity [60]. Using amphiphilic poly(vinyl alcohol) (PVA) aerogel as a substrate material for stabilizing metal single-atoms, Ma et al. [61] obtained a Zn/Mo dual single-atom nanomaterial supported on the macroscope aerogel (Zn/Mo DSAN-SMA) by soaking the aerogels with acetonitrile solutions of supramolecular coordination complexes/polyoxometalates (SCCs/POMs) followed by carbonization, which can be used as a novel nanozyme with ultra-long-term stability as a POD mimetic (Figure 5A). The constructed sensors can be used for the detection of glucose, AA, cholesterol, and H_2O_2 (Figure 5B). Theoretical calculations indicated that the Zn/Mo site is the main active center, and the synergistic effect between Zn and Mo atoms led to the superior activity of Zn/Mo DSAN-SMA. Achieving controlled synthesis and modulation of diatomic sites is essential for optimizing the performance of dual-atom nanomaterials (DANs). Due to the influence of geometry on the local electronic structure, the atomic sites at the edges are very different from those on the base surface of the supported materials in terms of electron density. The introduction of defects in the substrates is an effective way to increase the number of active sites at the edges while also facilitating material migration and the exposure of active sites. Kim et al. [62] designed a large number of defects on N-doped mesoporous carbon NPs using OH· generated by the decomposition of H_2O_2 under a hydrothermal process at 180 °C to etch the carbon-based support, and these defect edges provided anchor sites for Fe atoms (Figure 6A). Such edge sites exhibited significantly enhanced POD and oxidase (OXD)-like properties. Theoretical calculations suggested that the increased activity is due to the higher electron density of the N atoms at the edge sites, allowing for new reaction pathways at the edge sites (Figure 6B). Similar to noble metal-based SANs, modulating the metal coordination environment of non-noble metal-based SANs, such as the introduction of axial ligands or heteroatoms, can also affect the electronic structure of the active sites, thereby improving the catalytic activity as well as the specific recognition of the catalytic substrate [63,64], and the design of these SANs is also expected to be applied in the field of electrochemical sensors. A boron-doped Fe–N–C (FeBNC) nanozyme was developed by Jiao et al. [65] by mimicking the active sites of natural POD, in which the B atoms in the second coordination shell induced the electronic rearrangement of iron. The FeBNC nanozyme specifically enhanced the POD-like activity compared to the FeNC nanozyme. Axial nitrogen ligands play a crucial role in stabilizing the active structure and enhancing enzyme activity. By mimicking the structure of natural enzymes, a five-coordinated Fe-based single-atom nanozyme has been synthesized, displaying 7.64-fold higher POD-like activity than Fe–N_4 nanozyme [66] (Figure 7A). Theoretical calculations suggested that this reason is that Fe–N_5 molecules exhibit higher affinity for H_2O_2 and better activation ability (Figure 7B,C).
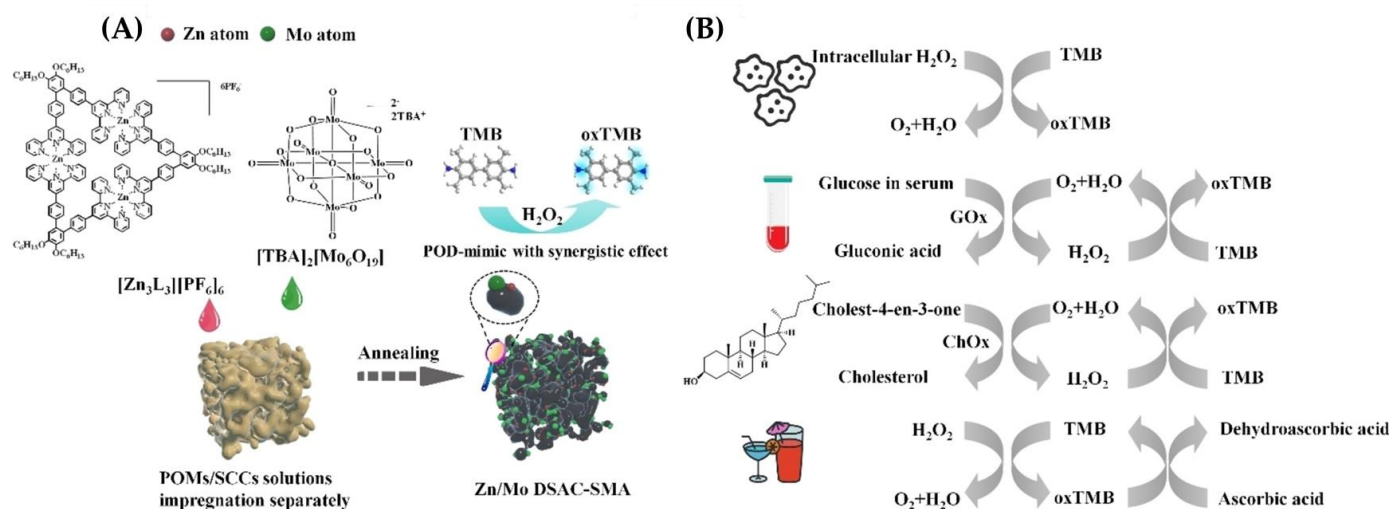
Figure 5. (**A**) Schematic illustration of the fabrication process of the confined Zn/Mo dual single-atom nanozyme loaded on PVA-based aerogel. (**B**) Versatile applications in intracellular H_2O_2 detection, glucose detection in serum, cholesterol determination, and AA in beverage detection [61]. Copyright 2022 with permission from Wiley.

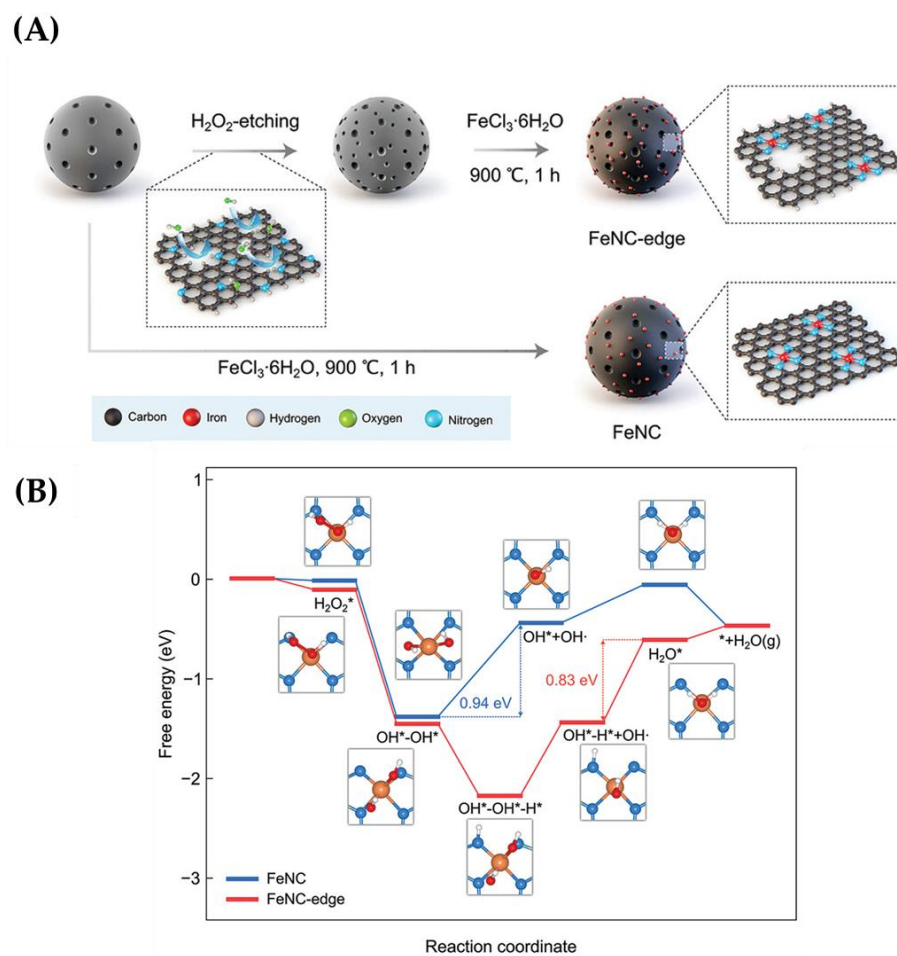**Figure 6.** (**A**) Schematic illustration of FeNC-edge synthesis. (**B**) Free energy diagram for the POD-like reaction of FeNC and FeNC-edge. Color code: Fe, orange; nitrogen, blue; oxygen, red; H, white [62]. Copyright 2023 with permission from Wiley.
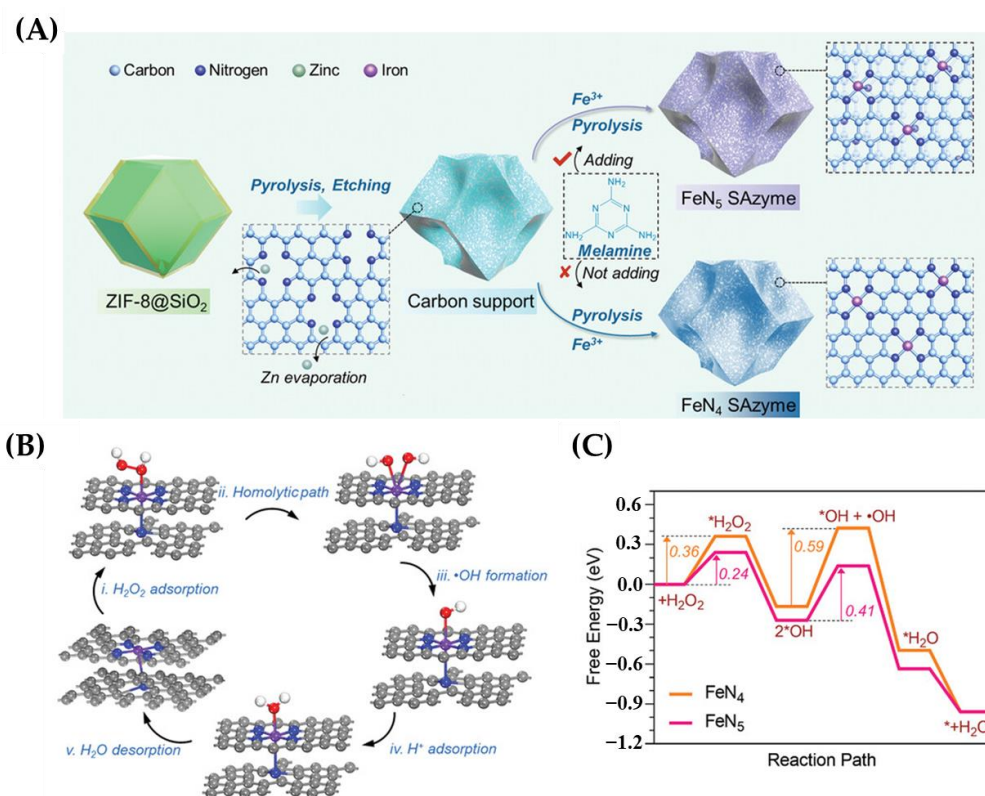
Figure 7. (**A**) Schematic illustration of the synthesis process for FeN$_5$ SAzyme. (**B**) Proposed catalytic mechanism for peroxidase-like reaction on FeN$_5$. (**C**) Corresponding free energy diagram for peroxidase-like reactions on FeN$_5$ and FeN$_4$ [66]. Copyright 2022 with permission from Wiley.

3. Types of SANs-Based Electrochemical Sensing

Integrating the virtues of SANs with electrochemical analytical methods has become a popular approach for constructing highly sensitive and selective analytical sensors, and the following section specifically describes the application of SANs in the fields of electrochemical sensing, electrochemiluminescent sensing, and photoelectrochemical sensing.

3.1. SANs-Based Electrochemical Sensing

Electrochemical analysis refers to a set of techniques used to study and analyze the behavior of chemical substances and processes, involving the measurement and interpretation of electrical properties such as current, potential, cuductivity, and so on, arising from chemical reactions occurring at the electrode interface. The use of SANs in electrochemical sensors offers numerous advantages, including enhanced sensitivity, selectivity, faster response times, stability, miniaturization, and energy efficiency because of the high catalytic activity and specificity of SANs. These characteristics make single-atom materials promising candidates for the development of advanced sensing devices with improved performance and wider practical applications.

The main class of electrochemical sensors constructed by SANs are those based on current analysis, that is, a certain voltage is applied and a corresponding current is generated by the redox reaction of the substance to be measured at the electrode through electrochemical catalysis, thus allowing quantitative analysis (Table 1). The amperometric method is currently a very popular method in electrochemical sensing. The four-electron pathway of ORR plays a very important role in electrochemical oxygen sensing, but the commonly used Pt/C catalysts for the analysis of oxygen in complex systems need to be improved due to the current influence of the H_2O_2 reduction reaction. A SAN with Co–N$_4$ as the active center was designed, which can effectively promote the four-electron ORR in a potential- and loading density-dependent manner under neutral conditions [67]. A

hydrophobic hexamine monomolecular layer was electrochemically applied to the carbon fiber microelectrode (CFE) surface by CV scanning, and then the Co–N$_4$/C catalyst was adsorbed onto the modified CFE via hydrophobic interactions. The CFE was implanted as a working electrode (WE) in the right cortex of the rat brain, and oxygen was effectively detected by a typical amperometric response. The weak interaction between H$_2$O$_2$ and the active sites led to its highly selective sensing of oxygen, thus realizing real-time specific sensing of oxygen in vivo. Li et al. [68] prepared a Fe-based SAN using two-dimensional nitrogen-doped graphene as a support. It possessed a larger specific surface area to ensure high loading of active sites than 1D carbon substrates. And the distance between adjacent active centers in the catalyst matched the -O–O- bridge adsorption mode, allowing the H$_2$O$_2$ reduction reaction to occur in a 2-electron transfer path with higher catalytic activity compared to the 1-electron path occurring in the 1D NW-loaded SAN. Fe–SAN/NW was modified onto GCE and then Nafion solution was deposited onto the sensor surface to obtain an electrochemical sensor for remarkably sensitive detection of H$_2$O$_2$, which can also be used for in situ monitoring of H$_2$O$_2$ release from cells. H$_2$O$_2$ was catalyzed by the Fe active centers on the electrode surface for reduction to produce water, and the current was linearly related to the H$_2$O$_2$ concentration. The introduction of synergistic components in SANs can optimize the electronic and geometric structure of metal atoms, which enables efficient electrochemical sensing. Aiming to improve the POD activity of SAN, Fe single atomic sites with carbon-encapsulated Fe$_3$C crystals (Fe$_3$C@C/Fe–N–C) were synergized by Wei et al. [69] to enhance the adsorption of H$_2$O$_2$ molecules on Fe sites by transferring electrons from Fe$_3$C@C to single atomic Fe sites. It was used to construct a hydrogen peroxide electrochemical sensor with a high sensitivity of 1225 μA/mM·cm^2 and a low detection limit of 0.26 μM. In addition to the amperometric method, differential pulse voltammetry (DPV) is one of the commonly used techniques, in which square pulses are applied to a linear potential sweep. An ultrasensitive dopamine (DA) electrochemical sensor has been constructed by doping Mn atoms on electrodeposited MOS$_2$ nanosheets (Mn–MoS$_2$) and using Mn–MoS$_2$ as WE [70]. DA was catalytically oxidized on the electrode surface, and the current measured using the DPV method increased with increasing DA concentration. In contrast to MoS$_2$, Mn–MoS$_2$ had higher selectivity and sensitivity for DA detection, with limits of detection (LOD) of 50 pM, 5 nM, and 50 nM in buffer, 10% serum, and artificial sweat, respectively. The Mn atoms took the place of Mo atoms in the MoS$_2$ lattice (Mn$_{Mo}$) or adsorb on Mo atoms (Mn$_{topMo}$), and the former was more energetically favorable compared to the latter. DA molecules were physisorbed on Mn$_{Mo}$, unlike chemisorption on Mn$_{topMo}$, where the former dominated at low DA concentrations and the latter dominated at high concentrations. There are also studies in which the linear sweep voltammetry (LSV) method was used for electrochemical quantification. Ding et al. [71] doped iron single atoms onto polypyrrole-derived carbon NW to synthesize Fe–N–C-based single-atomic site catalysts (Fe–SASC/NW), which featured Fe–N$_x$ structures that can mimic the active sites of heme enzymes. The electrochemical sensor constructed by modifying Fe–SASC/NW onto the electrode can achieve highly sensitive detection of H$_2$O$_2$, and the LSV results demonstrated that the Fe–SASC/NW modified electrode can produce a linear current response to H$_2$O$_2$ with a linear concentration range from 5.0×10^{-10} M to 0.5 M and a LOD of 46.35×10^{-9} M.

In some studies, potentiometric analysis is used, i.e., the potential difference between the WE and the reference electrode in the open circuit is recorded and used as the output signal for the quantitative analysis of chemical substances. Pan et al. [72] coupled SAN with galvanic redox potentiometry (GRP) for the detection of H$_2$S in living mouse brains. (Figure 8) GRP is achieved by constructing a " galvanic cell " that spontaneously forms a redox process with the substance to be measured and by recording the open-circuit potential (OCP) without an applied polarization voltage. To avoid other coexisting neurochemicals with similar redox potentials from affecting the H$_2$S detection, they constructed an electrochemical sensor with high selectivity for H$_2$S by hydrophobically adsorbing hollow carbon spheres loaded with single Ni atoms onto the electrode to promote electrochemical H$_2$S

oxidation at very low potentials, thus driving spontaneous bipolarization of a single carbon fiber. Almost no current flowed in the circuit during the measurement, so the process did not electrically affect or interfere with the nervous system.
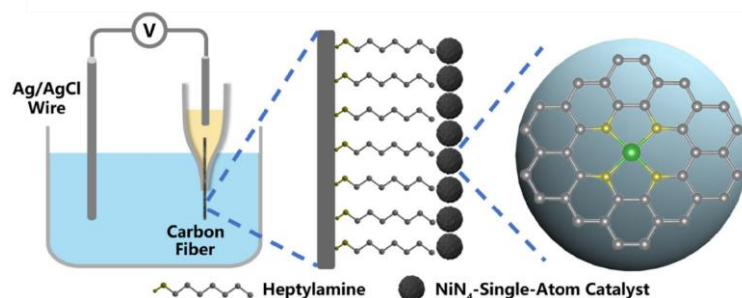

Figure 8. Schematic illustration of the NiN_4–SACs–GRP microsensor for H_2S sensing. The inner pole of the carbon fiber was immersed in an artificial cerebrospinal fluid (aCSF) solution containing 10 mM K_3Fe $(CN)_6$ and K_4Fe $(CN)_6$ (yellow). The outer pole of the carbon fiber was modified with NiN_4-SACs to catalyze the electrochemical oxidation of H_2S in bulk media (blue) [72]. Copyright © 2022 American Chemical Society.

Table 1. Summary of reported SANs-based electrochemical biosensors and applications.

SANs	Analyte	Sensitivity (μA mM^{-1})	Linear Range (μM)	LOD (μM)	Reference
Fe–SASC/NW	H_2O_2	-	5×10^{-4}~5×10^5	0.04635	[71]
$Fe_3C@C/Fe$–N–C	H_2O_2	1225 cm^{-2}	1~6000	0.26	[69]
Cu_1/C_3N_4	H_2O_2	0.155	-	-	[73]
Fe–SASC/G [1]	H_2O_2	3214.28 cm^{-2} 1785.71 cm^{-2}	10~920 920~7020	0.2	[68]
Fe Sas–N/C	H_2O_2	86.99 32.66 19.91	1~54 54~764 764~9664	0.34	[74]
Ni–SAC	H_2O_2	-	2×10^{-5}~2.22×10^4	6.87×10^{-6}	[75]
Se SA/NC	H_2O_2	403.9 cm^{-2}	40~1.11×10^4	18	[76]
Fe_1Se_1/NC	H_2O_2	1508.6 cm^{-2}	20~1.3×10^4	11.5	[77]
Co–N–C-800	H_2O_2 DA	943.9 cm^{-2} 979.6 cm^{-2}	0.3~1.0×10^6 0.06~1200	0.13 0.04	[78]
Ni–MoS_2	DA	-	1×10^{-6}~1000	1×10^{-6}	[79]
Ru–Ala [2]–C_3N_4	DA UA	0.083 0.033	0.06~490 0.5~2135	0.02 0.17	[80]
Ru_3/NC	DA UA	58 24	0.01~200 0.05~1000	0.033 0.01	[58]
Fe–N_5–SAC	DA UA	2150 2740	0.005~500 0.01~480	7 27	[25]
Pt_1/Cu@CuO NWs	glucose	852.163 cm^{-2}	0.01~5.18	3.6	[54]
NCA [3]–Co	glucose	7.8 1	0.5~1000 1000~6000	0.1	[27]
Pt_1/Ni_6Co_1LDHs [4]/NG [5]	glucose	273.78 cm^{-2}	100~2180	10	[81]
$Pt_1/Ni(OH)_2/NG$	glucose	220.75 cm^{-2}	10~2180	-	[82]
Ti–MOF [6]–Pt	thrombin	-	4×10^{-6}~0.2	1.3×10^{-6}	[83]
SANb–BCN [7]	NB	480.37 156.64	2~100 100~600	0.7	[84]

[1] G—graphene; [2] Ala—alanine; [3] NCA—N-doped carbon aerogel; [4] LDHs—layered double hydroxides; [5] NG—nitrogen-doped graphene; [6] MOF—metal-organic framework; [7] SANb-BCN—single-atom niobium-doped boron–carbon–nitrogen nanotubes.

3.2. SANs-Based Electrochemiluminescence Sensing

ECL consists of an electrochemical initiation step and an optical readout step and is a luminescence process resulting from the relaxation of electronically excited products to the ground state following an electrochemical reaction. It has been widely used in biomedical fields because it does not require an excitation light source, giving it a lower background compared to other optical methods, and is potential and spatially controlled. Combining the high activity and large surface area of SANs, SANs offer the advantages of enhanced ECL signal intensity, tunable emission properties, high stability, fast response time, selectivity and specificity, integration with nanostructures, and miniaturization. In addition, the performances of SANs can be enhanced by their controlled atomic structure and strong bonding interactions; as a result, the sensitivity and selectivity of SANs-based ECL sensors can be improved for a wide range of applications, such as biomedical diagnostics, environmental monitoring, and chemical analysis.

The sensitivity of ECL sensing is significantly related to the efficiency of photon generation; therefore, SANs can act as co-reaction accelerators by virtue of their high catalytic activities to effectively promote the generation of excited luminescent substances at the surface of the electrode. Luminol, a classical luminescent, has a low oxidation potential, which reduces interference from other reactions. There have been many studies using SANs to catalyze the generation of reactive oxygen species (ROS) from the co-reactant to achieve signal amplification. Gu et al. [56] modified the electrode with Fe-based SAN containing Fe-N_4 active sites, which showed better enhancement of ECL efficiency than nitrogen-doped carbon and Fe_3O_4 NPs. (Figure 9A,B) To verify the ECL signal enhancement mechanism, they added isopropanol (IPA) or benzoquinone (BQ) as ·OH and $O_2^{·-}$ radical scavengers, respectively, to the Fe–N–C–luminol system, and the significantly decreased luminescence signal proved that the SAN promoted the ECL reaction through the radical pathway. FeN_4 active sites catalyzed the generation of ROS from dissolved oxygen at the electrode surface, amplifying the ECL signal of luminol. Exploiting the fact that antioxidants can eliminate free radicals to inhibit ECL, a Trolox sensor was constructed with a linear range of detection from 0.8 μM to 1.0 mM (Figure 9C). To further investigate the ECL mechanism, they later also designed two carbon-supported nickel SANs with Ni–N_4 and Ni–N_2O_2 for catalytic ORR, demonstrating four- and two-electron pathways, respectively [85]. The results showed that the Ni–N_4 active site had a better enhancement of the ECL signal and that $O_2^{·-}$ was the main active intermediate species for the ECL reaction. The Ni–N_4/C–luminol ECL system was used to detect AA in the linear range of 70 μM to 350 nM. The plasma exciton effect, a collective oscillation of dense electrons, is capable of converting light energy into electronic excitation, and combining it with ECL is considered to be an efficient way to improve detection sensitivity. Au@SiO_2 and Fe–SAN were coupled by Bushira et al. [86] to enhance the ECL of the luminol-dissolved oxygen system by plasmon effect and construct sensitive and stable ECL sensors for the detection of DA, heme, and mercury (Hg^{2+}). The relationship between the cathodic ECL behavior of the luminol-oxygen system and the ORR electrocatalytic activity of SANs was examined by Xia et al. [87], and the results showed that the ECL intensity was positively correlated with the ORR catalytic activity. Two Fe-based SANs with different active sites, Fe–SAN and Fe–SAN(O), were designed, and enhanced luminescence signals were detected at the cathode without direct luminol electrochemical oxidation. Fe–SAN and Fe–SAN(O) generated electrocatalytic ORR via four-electron and two-electron pathways, respectively, and the difference in the electronic structure of the metal centers caused significant differences in the ECL signals. Among them, Fe-SAN with a $4e^-$-pathway tended to generate more kinds of ROS with stronger ECL intensity. This work achieved the tuning of the cathode ECL performance, and the ECL sensor constructed based on Fe–SAN had a detection limit of 0.10 nM for AA. Recently, some researchers have also employed SANs in the ECL system of $Ru(bpy)_3^{2+}$/$S_2O_8^{2-}$. Fe–SAN effectively activated $S_2O_8^{2-}$ to $SO_4^{·-}$ and significantly enhanced the cathodic ECL emission of $Ru(bpy)_3^{2+}$ [88].
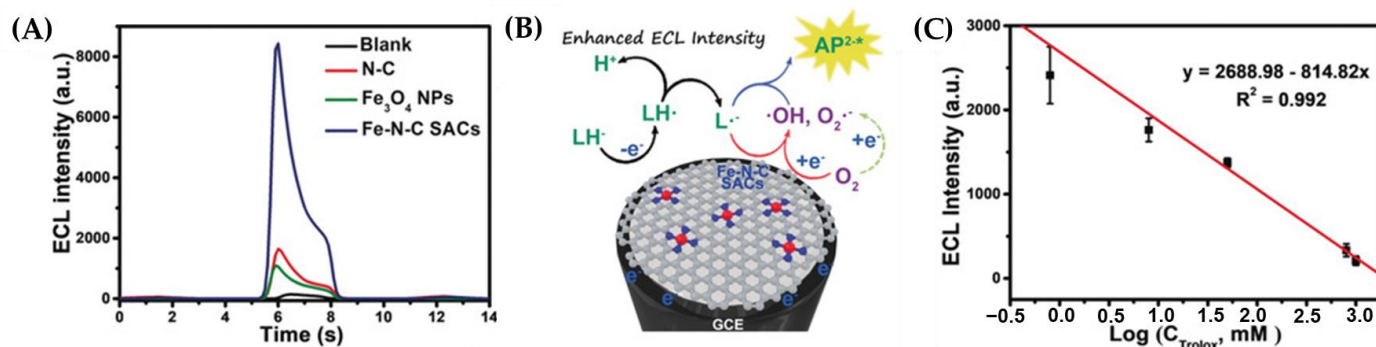
Figure 9. (**A**) ECL intensity of bare GCE and modified GCE with N–C, Fe_3O_4 NPs, and Fe–N–C SACs. (**B**) The mechanism of luminol–O_2 ECL systems with Fe–N–C SACs as coreactant accelerators. (**C**) The linear relationship between the Trolox concentration and ECL peak intensity [56]. Copyright 2019 with permission from Wiley.

SAN is not only able to act as a co-reaction accelerator to promote the generation of ROS but also as an ECL probe in some systems. Ma et al. [89] modified Ni SANs with polyethylene glycol (PEG) to enhance their hydrophilicity and promote catalyst dispersion in water, and the functionalized Ni SANs could be used as ECL probes to label biomolecules. They labeled phage recombinant cell-binding domains with PEGylated Ni SANs (Ni@PEG) for recognizing methicillin-resistant Staphylococcus aureus (MRSA) and modified porcine IgG as a capture molecule on GCE deposited with gold nanoparticle membranes to construct a sensor for MRSA with a detection limit of 25 CFU/mL. In addition to oxygen, SANs also have similar applications in the ECL system of Luminol/H_2O_2. By combining Cu–SAN and CdS quantum dots as a cathodic luminophore, Eu MOF-loaded isoluminol–Au NPs as an anodic luminophore, and modifying human epithelial protein 4 (HE4) Ab_2 and carbohydrate antigen 125 (CA125) Ab_2 on the two luminophores, respectively, a sandwich immunosensor was constructed for the simultaneous detection of two different markers [90]. CuSAN was used as a co-reaction accelerator to catalyze the generation of large amounts of $\cdot OH$ and $O_2^{\cdot-}$ from H_2O_2 to promote luminescence.

3.3. SANs-Based Photoelectrochemical Sensing

PEC is composed of two processes: photoelectric conversion and electrochemical processing. Firstly, the PEC active material is excited by absorbing photons under light irradiation, and the photogenerated carriers generate photovoltage or photocurrent through charge transfer and transmission, thus realizing photoelectric conversion. Then the photogenerated carriers are transferred to the loaded electrode or solid–liquid interface, and charge exchange occurs at the interface, completing the redox reaction and transforming the chemical information into electrical signals [3]. The development of PEC materials with high photoactivity by using the huge surface active sites of SANs to trigger unique surface reactions is crucial to improving the analytical performance of PEC sensors [91]. Single metal atoms can effectively modulate the energy band and electronic structure of semiconductor frameworks, thus improving their corresponding light trapping and charge transport behaviors. At the same time, single atoms can significantly accelerate interfacial redox reactions due to their high catalytic activity and thus reduce the aggregation of charge carriers.

A Pt-based SAN has been synthesized by anchoring Pt atoms on the surface of hollow CdS (HCdS–Pt_1) [92], which was used as a PEC sensing platform. The introduction of Pt_1 increased the carrier density, leading to higher PEC activity in HCdS–Pt_1 compared to HCdS and HCdS–PtNPs. A biomolecular sensor was constructed by encapsulating HRP and glucose oxidase (GOx) in DNA flowers (HRP and GOx-DFs) as recognition elements and exploiting the phenomenon that target exosome-enriched HRP and GOx-DFs irreversibly bio-etch HCdS–Pt_1 in the presence of glucose, thereby causing changes in the photocurrent

intensity. Since Pt is an ideal PEC photoactive material and its strong ability to provide electrons through chemical Pt–S interactions with CdS provides high photocurrent signal output, Qin et al. [93] prepared Pt single atoms dispersed on CdS nanorods (Pt SAs–CdS) that exhibited favorable ability for the separation of electron-hole pairs and constructed a prostate-specific antigen (PSA) sensing platform. The secondary antibodies (Ab$_2$) were labeled with CuO, and under acidic conditions, CuO NPs can dissociate into Cu^{2+} ions, which changed the PEC properties of Pt SAs–CdS photoelectrodes by reacting with them. Therefore, the addition of PSA led to a decrease in photocurrents, and the enzyme-free PEC immunosensor constructed using this principle was used to detect PSA in the linear range of 5 pg/mL to 10 ng/mL with a detection limit of 0.92 pg/mL. To improve the photoactivity and stability of pure CdS loaded with single atoms, CdS has been replaced with Zn$_{0.5}$Cd$_{0.5}$S, which can improve the photogenerated holes/electrons mobility, thus reducing the bulk hole-electron complex and the oxidation of divalent sulfide ions by photogenerated holes [94]. The constructed PEC sensor had a detection limit of 0.22 pg/mL for PSA. Except for Pt, the very commonly used Fe-based SAN can also improve PEC sensing performance by promoting interfacial reactions in a typical p-type semiconductor of Cu$_2$O. Fe SANs have also been integrated with Cu$_2$O/Ti$_3$C$_2$T$_x$ by Qin et al. [31] to construct a highly sensitive PEC biosensor by enhancing the ORR catalytic activity at the interface and thus the PEC signal (Figure 10). Fe SANs were also found to exhibit superior POD activity and could catalyze the oxidation of 4-chloro-1-naphthol (4-CN) on the photoelectrode surface to form insoluble precipitates and thus weaken the PEC signal. Since acetylcholinesterase (AChE) was able to catalyze the hydrolysis of acetylcholine (ACh) to form acetic acid, which led to a change in the pH value of the solution, thus affecting the POD activity of Fe SANs/Ti$_3$C$_2$T$_x$/Cu$_2$O, the PEC sensor constructed based on this principle provided highly sensitive detection of AChE activity and organophosphorus pesticides (OPs, AChE inhibitors). TiO$_2$, as a semiconductor with chemical stability and strong light absorption ability, when combined with gC$_3$N$_4$ to form a heterojunction, can achieve effective separation of carriers. Bott-Neto et al. [30] modified TiO$_2$ and graphitic carbon nitride anchored with nickel single atoms (Ni–gC$_3$N$_4$) to form heterojunctions on screen-printed carbon electrodes (SPCEs) and functionalized TiO$_2$ with electrodeposited aryl diazonium salts to anchor antibodies and facilitate the separation of charge carriers. A miniaturized 3D-printed PEC device that can detect PSA under visible LED light irradiation with good stability and a detection limit of 0.06 fg/mL was constructed using the synergy of these three materials.
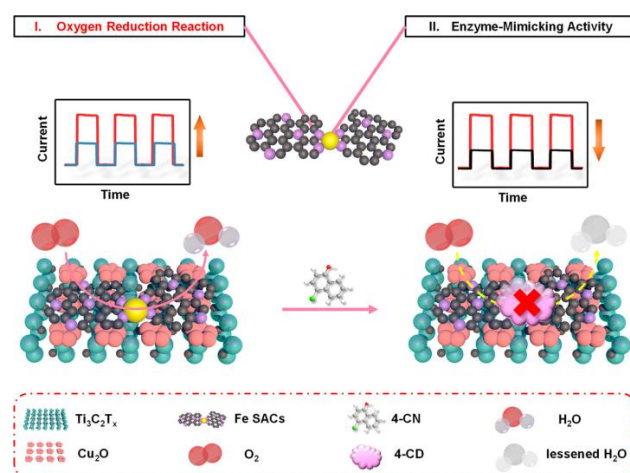

Figure 10. Operation of the Fe SACs/Cu$_2$O/Ti$_3$C$_2$T$_x$-based PEC analytical platform. Schematic illustration depicting the principle of the PEC analytical platform with the expected change in photocurrent profile due to the bifunctional Fe SACs [31]. Copyright © 2022 American Chemical Society.

4. Applications of SANs in Analytical Chemistry

SANs-based sensors have been used in a wide range of analytical applications. Some trace biological and environmental samples require high sensitivity for detection, and SANs have shown great applicational values in electrochemical sensing of biomolecules and environmental contaminants in vivo and in vitro with their powerful structural and performance advantages. The following section focuses on their application in environmental and biochemical analysis.

4.1. Applications of SANs in Biochemical Analysis

The detection of some signaling molecules in living organisms is of crucial importance for the prevention and diagnosis of diseases. The development of SANs has led to non-negligible progress in this research area of constructing highly sensitive biosensing platforms [27,71,78]. The analysis of endogenous substances generated by cells is a typical class of application. For example, NO, as an endogenous cellular substance associated with a variety of physiological and pathological conditions, requires high sensitivity and transient recording capability on the sensor. A Ni-based SAN has been designed by anchoring Ni atoms on nitrogen-doped hollow carbon spheres (Ni SANs/N–C) by Zhou et al. [95], which can effectively catalyze the electrochemical oxidation of NO, and constructed a stretchable electrochemical sensor by confining Ni SANs/N–C on a flexible dimethylsiloxane (PDMS) substrate (Figure 11A,B). This sensor had good biocompatibility, realized real-time detection of NO release from endothelial cells during drug and traction stimulation, and also provided a new idea for the design of sensing platforms for chemical signals in the environment of living cells. H_2O_2, an important representative of ROS, is generated by intracellular oxygen metabolism and plays a crucial role in stimulating cell proliferation, differentiation, and migration. The construction of sensors that can provide accurate, real-time detection of H_2O_2 produced by living cells has been an important topic. Liang et al. [74] constructed an electrochemical sensor for H_2O_2 detection with a detection limit of 0.34 μM by modifying Fe SAs–N/C prepared by high-temperature calcination carbonization of hemin@zeolitic imidazolate framework-8 (hemin@ZIF-8) on GCE and exploiting the POD activity of Fe–N_x active sites.
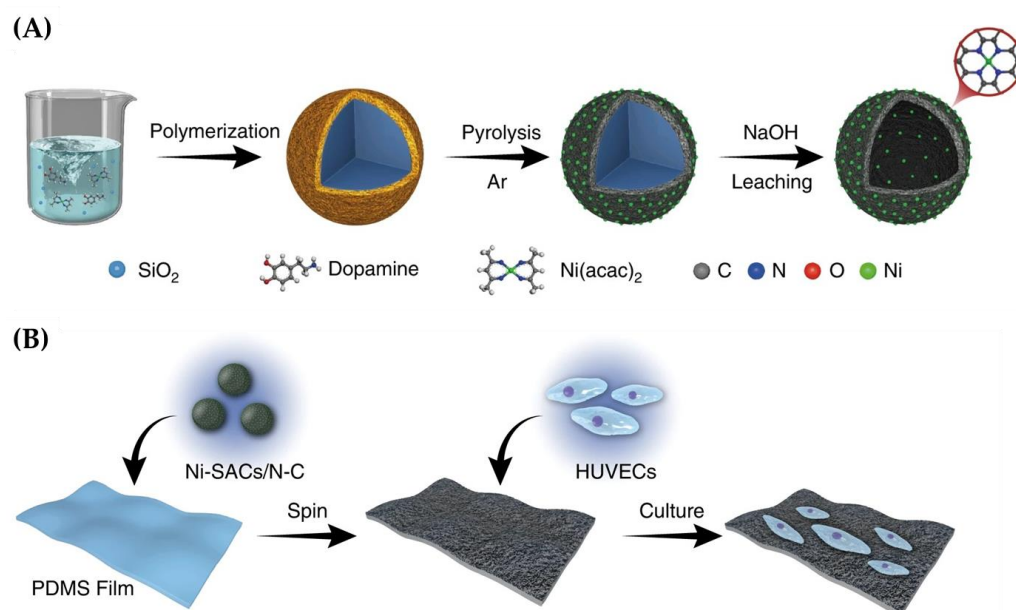
(A)

(B)

Figure 11. (**A**) Schematic illustration of the synthesis of Ni SACs/N–C. (**B**) Schematic illustration of the fabrication of Ni SACs/N–C-based stretchable sensors for NO sensing and HUVEC culturing [95]. Copyright © 2020, Nature, open access.

Achieving in vivo monitoring of neurochemicals and then studying brain function is crucial and challenging. An enzyme-based electrochemical sensor for glucose has been designed using the property that Co-based SAN can catalyze the oxidation of H_2O_2 at low potentials [96], which in turn enabled online monitoring of glucose in rat brain microdialysate. This sensor inherited the superiority of electrochemical analysis and SANs, with a good response to glucose and no interference from other electroactive substances. This work provided a new idea for in vivo analysis that can also be applied to the analysis of other chemicals. An effective method for the detection of H_2O_2 is to use a hydrogen peroxide reduction reaction (HPRR), but the detection process is often disturbed by ORR. To improve the selectivity of H_2O_2 detection. Gao et al. [73] dispersed single Cu atoms on mesoporous graphitic carbon nitride through the impregnation method, and the obtained Cu_1/C_3N_4 was proved to have better HPRR electrocatalytic performance than ORR in neutral media by theoretical calculation. Based on this, a microsensor with high selectivity for hydrogen peroxide was designed and implanted into the rat brain to achieve selective monitoring of H_2O_2 fluctuations in vivo.

In addition, electrochemical sensors based on SANs have also been used for some other biological small-molecule detection or immunoassays. To address the problem that the detection of UA in serum is difficult to achieve an ultra-wide linear range and an ultra-low detection limit, and the detection mechanism is unclear, an electrochemical UA sensor has been developed by Hu et al. [97], relying on a Co single-atom nanozyme (A–Co–NG) for the first time. These Co atoms in the prepared A–Co–NG nanozyme were coordinated to 3.4 N atoms on average in the form of Co^{2+}. The detection range of this A–Co–NG sensor was 0.4 to 41,950 μM, and the detection limit was 33.3 ± 0.024 nm, which was significantly better than the previously reported sensors based on various nanomaterials. This work provided excellent material for realizing a UA sensor with a wide detection range and low detection limit, which met the need for practical diagnosis and provided new ideas to guide the exploration of other biosensing processes. An electrochemical sensor that can detect DA and UA simultaneously was designed by Xie et al. [80] through dispersing Ru atoms on a C_3N_4 substrate, with linear ranges of 0.06 to 490 μM and 0.5 to 2135 μM for DA and UA, respectively, and detection limits of 20 and 170 nM, respectively. Furthermore, an immunosensor for the detection of PSA was also constructed by inducing PEC signal inhibition by CuO NPs-labeled sandwich immunocomplexes.

4.2. Applications of SANs in Environmental Analysis

SANs have also been applied to the detection of some heavy metal ions in environmental samples. For instance, an ultrasensitive electrochemical sensor for the heavy metal ion Pb^{2+} has been designed by Zhou et al. [98] through doping Mn atoms into MoS_2 nanosheets, in which Mn atoms took the place of some Mo atoms. The introduction of Mn atoms caused lattice destabilization and sulfur vacancies (V_S) on the one hand and phase changes on the other, adding another 1T-phase to $Mn–MoS_2$ compared with pure MoS_2 containing only 2H-phase. Defect- and phase-engineering enabled $Mn–MoS_2$ not only to have excellent electronic properties but also to form Pb–S bonds with lead ions, which significantly promoted in situ catalytic redox reactions. Yao et al. [99] synthesized a homogeneous dodecahedral N-doped carbon modified by a Fe–N–C SAE and modified it onto the gate electrode of the solution-gated graphene transistor (SGGT) to construct an electrochemical sensor for real-time monitoring of Hg^{2+} in environmental samples. (Figure 12) Combining the excellent electrocatalytic performance of Fe–N–C SAE with the high signal amplification efficiency of SGGT, this sensor has good sensitivity and selectivity for Hg^{2+} with a detection limit as low as 1 nM. Li et al. [100] realized that Co-based SANs have great superiority in the field of detection of trace-level As(III). The Co atoms anchored on the N-doped carbon substrate were active sites for catalyzing the reduction reaction of H_3AsO_3 with the formation of Co–O hybridization bonds, which resulted in a Co SAN that was more favorable than Co NPs in terms of both kinetics and thermodynamics. The As (III) electrochemical sensor constructed based on Co SAN had a good selectivity and a

sensitivity of 11.44 μA ppb^{-1}. Some other environmental pollutants, such as nitrobenzene (NB) and hydroquinone (HQ), also have problems in terms of sensitivity and selectivity for detection, and the development of SAN provides a new idea for them. Four different scales of Mo-based nanostructures were prepared by Cong et al. [101], including Mo$_2$C NPs, Mo$_2$C nanodots, Mo nanoclusters, and Mo single atoms, on N, P, and O co-doped carbon substrates to compare their performance for electrochemical detection of HQ. The results showed that Mo single atoms exhibited the most sensitive results with a wide linear range (0.02 to 200 μM), a low detection limit (0.005 μM), and good anti-interference ability. Nb SAN has been prepared by Li et al. [84] using boron–carbon–nitrogen nanotubes as supports and modified onto GCE for the construction of electrochemical sensors for NB. Compared with bare GCE, SANb–BCN/ GCE for catalytic reduction reactions exhibited higher current intensity and could achieve detection limits as low as 0.70 mM, which was able to be used for the detection of NB in water samples. They also tested the anti-interference ability of the sensor using various inorganic and organic substances and found little effect on the detection signal, indicating a high specificity of the sensor for NB. Luo et al. [102] applied the ORR activity of the Ir SAN catalyst to electrochemical detection. They achieved the monitoring of AChE activity by exploiting the inhibitory effect of thiocholine (TCh) on the ORR activity of Ir–N$_x$ sites, and the AChE–Ir SAN-based biosensor can be used to detect OPs in environmental samples. The linear range of OPs detection was 0.5 to 500 ng mL^{-1}, with a low detection limit of 0.17 ng mL^{-1}.
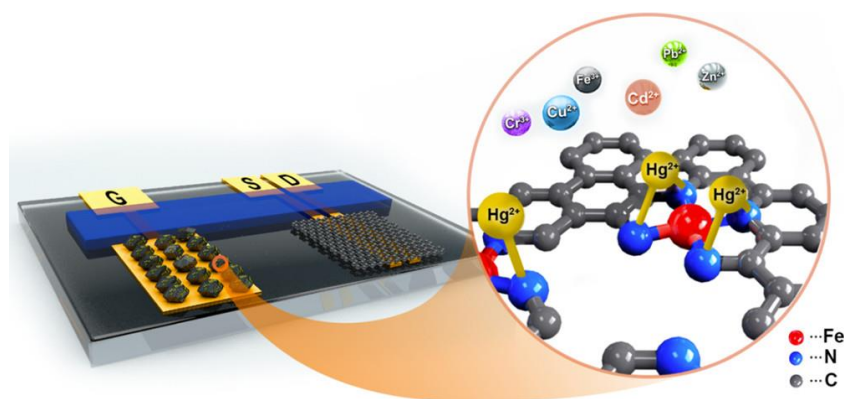

Figure 12. Schematic diagram of a solution-gated graphene transistor (SGGT) based on the Fe–N–C SAE and Cs/Au-modified gate electrode for the detection of Hg^{2+}. D, S, and G represent the drain, source, and gate electrodes, respectively [99]. Copyright © 2020 American Chemical Society.

5. Summary and Outlook

In this review, we first introduced the structural characteristics of SANs and the advantages that exist compared to conventional nanomaterials. Then, we highlight the progress made by researchers in recent years in tuning and optimizing the composition and structure of the active sites of SANs to improve catalytic performance, classified according to noble and non-noble metals, where the main approaches include the synergy of two or three metal atoms and the tuning of the coordination environment of metal atoms. Recent advances in the application of SANs in electrochemical sensing were also presented, including three types of sensing: electrochemical sensors, ECL sensors, and PEC sensors. Finally, the practical applications of SANs were presented according to the classification of biochemical and environmental analysis, which are promising for application in the sensitive detection of signaling molecules in living organisms and in vitro, as well as environmental pollutants. However, there are still some problems with SANs for applications in electrochemical sensors.

Firstly, SANs still face important challenges in their synthesis. Traditional synthesis methods still have difficulty achieving the desired metal loading, which hinders their large-scale application in practical production and is unfavorable to their application in the construction of highly sensitive sensors. There is a need to continue to develop new

synthesis methods that should ensure high metal loading while avoiding the aggregation of metal atoms into clusters or NPs. The dispersion of the metal is also very importantly related to the interaction between the metal and the support, so further search for suitable supports and optimization of their surface properties to make them more suitable for anchoring single metal atoms are needed. In addition to this, the active sites of some SANs may be encapsulated in the supports, which greatly reduces the utilization of the atoms. Ultrathin, ultrasmall supports such as carbon dots and monolayer 2D nanomaterials appear to increase the exposure of metal atoms significantly over bulk materials.

Secondly, the performance of SANs for biosensing still needs to be further optimized. The catalytic activity and specificity of SANs are far less than those of biological enzymes, so the synthesis of SANs with better performance needs to be realized through the precise analysis of the electronic structure and coordination environment of metal atoms to understand the structure-function relationship. Moreover, SANs still have a series of problems in terms of biocompatibility, targeting, and stability that need to be considered for bioanalytical applications, especially in vivo analysis.

Third, the application of SANs in wearable sensors is yet to be developed. Wearable sensors are powerful tools to monitor human health, but one of the major problems they are currently facing is the fast energy consumption due to miniaturized batteries, which prevents continuous monitoring for a long period of time. The development of wearable self-powered sensors is the most effective way to address this problem, and the key to it is to design a continuous and efficient power supply. Due to the excellent performance of SANs in catalysis, some researchers have already used SANs to construct self-powered sensors, such as using a SAN as the ORR catalyst for zinc-air batteries, which provided long-term stability and high power density and can be utilized for sensitive detection of glucose when integrated with glucose oxidase [103]. Recent work has also combined a SAN with enzymatic activity with photoactive materials to construct highly active PEC fuel cells that can be used for long-term and sensitive electrochemical sensing [104]. Because fuel cells and metal-air batteries are efficient sources of power supply in self-powered systems, coupled with the fact that SANs have shown great potential in catalyzing ORR, one of the two half-reactions essential to these two novel energy storage and conversion systems, SANs will surely play an indispensable role for self-powered sensors in the future.

In the future, with a further understanding of the conformational relationships and catalytic mechanisms of SANs, we believe that SANs will have great potential in the field of sensing.

Institutional Review Board Statement: The study did not require ethical approval.

Informed Consent Statement: This study did not involve humans.

Conflicts of Interest: The authors declare no conflict of interest.

References

1. Zheng, W. Single-Atom Materials as Electrochemical Sensors: Sensitivity, Selectivity, and Stability. *Anal. Sens.* **2022**, *3*, e20220007. [CrossRef]
2. Li, H.Y.; Qi, H.J.; Chang, J.F.; Gai, P.P.; Li, F. Recent progress in homogeneous electrochemical sensors and their designs and applications. *Trac-Trends Anal. Chem.* **2022**, *156*, 116712. [CrossRef]
3. Chen, Y.; Jiao, L.; Yan, H.; Xu, W.; Wu, Y.; Zheng, L.; Gu, W.; Zhu, C. Fe-N-C Single-Atom Catalyst Coupling with Pt Clusters Boosts Peroxidase-like Activity for Cascade-Amplified Colorimetric Immunoassay. *Anal. Chem.* **2021**, *93*, 12353–12359. [CrossRef] [PubMed]
4. Jiao, L.; Xu, W.; Wu, Y.; Wang, H.; Hu, L.; Gu, W.; Zhu, C. On the Road from Single-Atom Materials to Highly Sensitive Electrochemical Sensing and Biosensing. *Anal. Chem.* **2023**, *95*, 433–443. [CrossRef]
5. Chang, B.; Zhang, L.; Wu, S.; Sun, Z.; Cheng, Z. Engineering single-atom catalysts toward biomedical applications. *Chem. Soc. Rev.* **2022**, *51*, 3688–3734. [CrossRef] [PubMed]

6. Qiao, B.; Wang, A.; Yang, X.; Allard, L.F.; Jiang, Z.; Cui, Y.; Liu, J.; Li, J.; Zhang, T. Single-atom catalysis of CO oxidation using Pt_1/FeOx. *Nat. Chem.* **2011**, *3*, 634–641. [CrossRef] [PubMed]

7. Chen, Y.J.; Ji, S.F.; Chen, C.; Peng, Q.; Wang, D.S.; Li, Y.D. Single-Atom Catalysts: Synthetic Strategies and Electrochemical Applications. *Joule* **2018**, *2*, 1242–1264. [CrossRef]

8. Huang, Z.; Sun, X.; Wang, P.; Wan, H. Emerging single-atom catalysts in electrochemical biosensing. *View* **2023**, *4*, 20220058. [CrossRef]

9. Tajik, S.; Dourandish, Z.; Garkani Nejad, F.; Beitollahi, H.; Afshar, A.A.; Jahani, P.M.; Di Bartolomeo, A. Review—Single-Atom Catalysts as Promising Candidates for Electrochemical Applications. *J. Electrochem. Soc.* **2022**, *169*, 046504. [CrossRef]

10. Wang, A.Q.; Li, J.; Zhang, T. Heterogeneous single-atom catalysis. *Nat. Rev. Chem.* **2018**, *2*, 65–81. [CrossRef]

11. Wang, P.; Ren, Y.; Wang, R.; Zhang, P.; Ding, M.; Li, C.; Zhao, D.; Qian, Z.; Zhang, Z.; Zhang, L.; et al. Atomically dispersed cobalt catalyst anchored on nitrogen-doped carbon nanosheets for lithium-oxygen batteries. *Nat. Commun.* **2020**, *11*, 1576. [CrossRef]

12. Xia, C.; Qiu, Y.; Xia, Y.; Zhu, P.; King, G.; Zhang, X.; Wu, Z.; Kim, J.Y.T.; Cullen, D.A.; Zheng, D.; et al. General synthesis of single-atom catalysts with high metal loading using graphene quantum dots. *Nat. Chem.* **2021**, *13*, 887–894. [CrossRef]

13. Ran, L.; Li, Z.; Ran, B.; Cao, J.; Zhao, Y.; Shao, T.; Song, Y.; Leung, M.K.H.; Sun, L.; Hou, J. Engineering Single-Atom Active Sites on Covalent Organic Frameworks for Boosting CO_2 Photoreduction. *J. Am. Chem. Soc.* **2022**, *144*, 17097–17109. [CrossRef]

14. Qin, L.; Gan, J.; Niu, D.; Cao, Y.; Duan, X.; Qin, X.; Zhang, H.; Jiang, Z.; Jiang, Y.; Dai, S.; et al. Interfacial-confined coordination to single-atom nanotherapeutics. *Nat. Commun.* **2022**, *13*, 91. [CrossRef] [PubMed]

15. Zhang, E.; Tao, L.; An, J.; Zhang, J.; Meng, L.; Zheng, X.; Wang, Y.; Li, N.; Du, S.; Zhang, J.; et al. Engineering the Local Atomic Environments of Indium Single-Atom Catalysts for Efficient Electrochemical Production of Hydrogen Peroxide. *Angew. Chem. Int. Ed. Engl.* **2022**, *61*, e202117347. [CrossRef] [PubMed]

16. Yanan, S.; Xiaoguang, D.; Shaobin, W.; Qinyan, Y.; Baoyu, G.; Xing, X. Carbon-based single atom catalyst: Synthesis, characterization, DFT calculations. *Chin. Chem. Lett.* **2021**, *33*, 663–673. [CrossRef]

17. Chen, J.; Kang, Y.; Zhang, W.; Zhang, Z.; Chen, Y.; Yang, Y.; Duan, L.; Li, Y.; Li, W. Lattice-Confined Single-Atom Fe_1S_x on Mesoporous TiO_2 for Boosting Ambient Electrocatalytic N_2 Reduction Reaction. *Angew. Chem. Int. Ed. Engl.* **2022**, *61*, e202203022. [CrossRef] [PubMed]

18. Jiang, Z.; Tian, M.; Jing, M.; Chai, S.; Jian, Y.; Chen, C.; Douthwaite, M.; Zheng, L.; Ma, M.; Song, W.; et al. Modulating the Electronic Metal-Support Interactions in Single-Atom Pt_1-CuO Catalyst for Boosting Acetone Oxidation. *Angew. Chem. Int. Ed. Engl.* **2022**, *61*, e202200763. [CrossRef] [PubMed]

19. Kuai, L.; Liu, L.; Tao, Q.; Yu, N.; Kan, E.; Sun, N.; Liu, S.; Geng, B. High-Areal Density Single-Atoms/Metal Oxide Nanosheets: A Micro-Gas Blasting Synthesis and Superior Catalytic Properties. *Angew. Chem. Int. Ed. Engl.* **2022**, *61*, e202212338. [CrossRef] [PubMed]

20. Meza, E.; Diaz, R.E.; Li, C.W. Solution-Phase Activation and Functionalization of Colloidal WS_2 Nanosheets with Ni Single Atoms. *ACS Nano* **2020**, *14*, 2238–2247. [CrossRef] [PubMed]

21. Yang, Y.; Song, R.; Fan, X.; Liu, Y.; Kong, N.; Lin, H.; Li, Y. A mechanistic study of selective propane dehydrogenations on MoS_2 supported single Fe atoms. *Chin. Chem. Lett.* **2022**, *34*, 107257. [CrossRef]

22. Zhang, J.; Xu, X.; Yang, L.; Cheng, D.; Cao, D. Single-Atom Ru Doping Induced Phase Transition of MoS_2 and S Vacancy for Hydrogen Evolution Reaction. *Small Methods* **2019**, *3*, 1900653. [CrossRef]

23. Peng, Y.; Geng, Z.; Zhao, S.; Wang, L.; Li, H.; Wang, X.; Zheng, X.; Zhu, J.; Li, Z.; Si, R.; et al. Pt Single Atoms Embedded in the Surface of Ni Nanocrystals as Highly Active Catalysts for Selective Hydrogenation of Nitro Compounds. *Nano Lett.* **2018**, *18*, 3785–3791. [CrossRef] [PubMed]

24. Pei, G.X.; Liu, X.Y.; Yang, X.F.; Zhang, L.L.; Wang, A.Q.; Li, L.; Wang, H.; Wang, X.D.; Zhang, T. Performance of Cu-Alloyed Pd Single-Atom Catalyst for Semihydrogenation of Acetylene under Simulated Front-End Conditions. *Acs Catal.* **2017**, *7*, 1491–1500. [CrossRef]

25. Bushira, F.A.; Kitte, S.A.; Li, H.; Zheng, L.; Wang, P.; Jin, Y. Enzyme-like Fe-N_5 single atom catalyst for simultaneous electrochemical detection of dopamine and uric acid. *J. Electroanal. Chem.* **2022**, *904*, 115956. [CrossRef]

26. Liang, W.; Gao, M.; Li, Y.; Tong, Y.; Ye, B.C. Single-atom electrocatalysts templated by MOF for determination of levodopa. *Talanta* **2021**, *225*, 122042. [CrossRef]

27. Song, Y.Y.; He, T.; Zhang, Y.L.; Yin, C.Y.; Chen, Y.; Liu, Q.M.; Zhang, Y.; Chen, S.W. Cobalt single atom sites in carbon aerogels for ultrasensitive enzyme-free electrochemical detection of glucose. *J. Electroanal. Chem.* **2022**, *906*, 116024. [CrossRef]

28. Bushira, F.A.; Wang, P.; Wang, Y.; Hou, S.; Diao, X.; Li, H.; Zheng, L.; Jin, Y. Plasmon-Boosted Fe, Co Dual Single-Atom Catalysts for Ultrasensitive Luminol-Dissolved O_2 Electrochemiluminescence Detection of Prostate-Specific Antigen. *Anal. Chem.* **2022**, *94*, 9758–9765. [CrossRef]

29. Gu, W.; Wang, X.; Xi, M.; Wei, X.; Jiao, L.; Qin, Y.; Huang, J.; Cui, X.; Zheng, L.; Hu, L.; et al. Single-Atom Iron Enables Strong Low-Triggering-Potential Luminol Cathodic Electrochemiluminescence. *Anal. Chem.* **2022**, *94*, 9459–9465. [CrossRef]

30. Bott-Neto, J.L.; Martins, T.S.; Buscaglia, L.A.; Machado, S.A.S.; Oliveira, O.N., Jr. Photocatalysis of TiO_2 Sensitized with Graphitic Carbon Nitride and Electrodeposited Aryl Diazonium on Screen-Printed Electrodes to Detect Prostate Specific Antigen under Visible Light. *ACS Appl. Mater. Interfaces* **2022**, *14*, 22114–22121. [CrossRef] [PubMed]

31. Qin, Y.; Wen, J.; Wang, X.; Jiao, L.; Wei, X.; Wang, H.; Li, J.; Liu, M.; Zheng, L.; Hu, L.; et al. Iron Single-Atom Catalysts Boost Photoelectrochemical Detection by Integrating Interfacial Oxygen Reduction and Enzyme-Mimicking Activity. *ACS Nano* **2022**, *16*, 2997–3007. [CrossRef] [PubMed]

32. Zhao, L.; Qin, X.; Zhang, X.; Cai, X.; Huang, F.; Jia, Z.; Diao, J.; Xiao, D.; Jiang, Z.; Lu, R.; et al. A Magnetically Separable Pd Single-Atom Catalyst for Efficient Selective Hydrogenation of Phenylacetylene. *Adv. Mater.* **2022**, *34*, e2110455. [CrossRef] [PubMed]

33. Ji, K.; Xu, M.; Xu, S.M.; Wang, Y.; Ge, R.; Hu, X.; Sun, X.; Duan, H. Electrocatalytic Hydrogenation of 5-Hydroxymethylfurfural Promoted by a Ru$_1$Cu Single-Atom Alloy Catalyst. *Angew. Chem. Int. Ed. Engl.* **2022**, *61*, e202209849. [CrossRef]

34. Zheng, K.; Li, Y.; Liu, B.; Jiang, F.; Xu, Y.; Liu, X. Ti-doped CeO$_2$ Stabilized Single-Atom Rhodium Catalyst for Selective and Stable CO$_2$ Hydrogenation to Ethanol. *Angew. Chem. Int. Ed. Engl.* **2022**, *61*, e202210991. [CrossRef]

35. Zou, R.; Xie, R.; Peng, Y.; Guan, W.; Lin, Y.; Lu, C. Ag-O-Co Interface Modulation-Amplified Luminol Cathodic Electrogenerated Chemiluminescence. *Anal. Chem.* **2022**, *94*, 4813–4820. [CrossRef] [PubMed]

36. Li, X.; Wang, Z.; Tian, Y.; Li, X.; Cai, Q.; Zhao, J. Single-atom rhodium anchored on S-doped black phosphorene as a promising bifunctional electrocatalyst for overall water splitting. *Chin. Chem. Lett.* **2022**, *354*, 107812. [CrossRef]

37. Xu, J.; Xu, H.; Dong, A.; Zhang, H.; Zhou, Y.; Dong, H.; Tang, B.; Liu, Y.; Zhang, L.; Liu, X.; et al. Strong Electronic Metal-Support Interaction between Iridium Single Atoms and a WO$_3$ Support Promotes Highly Efficient and Robust CO$_2$ Cycloaddition. *Adv. Mater.* **2022**, *34*, e2206991. [CrossRef] [PubMed]

38. Shangguan, Y.; Zhou, Y.; Zheng, R.; Feng, X.; Ge, Q.; Wang, R.; Yang, D.; Wei, W.; Wu, X.; Lin, J.; et al. Bandgap engineering of tetragonal phase CuFeS$_2$ quantum dots via mixed-valence single-atomic Ag decoration for synergistic Cr(VI) reduction and RhB degradation. *Chin. Chem. Lett.* **2021**, *32*, 3450–3456. [CrossRef]

39. Yan, P.; Shu, S.; Shi, X.; Li, J. Promotion effect of Au single-atom support graphene for CO oxidation. *Chin. Chem. Lett.* **2022**, *33*, 4822–4827. [CrossRef]

40. Peng, L.; Yang, J.; Yang, Y.; Qian, F.; Wang, Q.; Sun-Waterhouse, D.; Shang, L.; Zhang, T.; Waterhouse, G.I.N. Mesopore-Rich Fe-N-C Catalyst with FeN$_4$-O-NC Single-Atom Sites Delivers Remarkable Oxygen Reduction Reaction Performance in Alkaline Media. *Adv. Mater.* **2022**, *34*, e2202544. [CrossRef]

41. Cai, X.; Ma, F.; Jiang, J.; Yang, X.; Zhang, Z.; Jian, Z.; Liang, M.; Li, P.; Yu, L. Fe-N-C single-atom nanozyme for ultrasensitive, on-site and multiplex detection of mycotoxins using lateral flow immunoassay. *J. Hazard. Mater.* **2023**, *441*, 129853. [CrossRef] [PubMed]

42. Du, Z.; Chen, X.; Hu, W.; Chuang, C.; Xie, S.; Hu, A.; Yan, W.; Kong, X.; Wu, X.; Ji, H.; et al. Cobalt in Nitrogen-Doped Graphene as Single-Atom Catalyst for High-Sulfur Content Lithium-Sulfur Batteries. *J. Am. Chem. Soc.* **2019**, *141*, 3977–3985. [CrossRef] [PubMed]

43. Sun, H.; Liu, J. Carbon-supported CoS$_4$-C single-atom nanozyme for dramatic improvement in CO$_2$ electroreduction to HCOOH: A DFT study combined with hybrid solvation model. *Chin. Chem. Lett.* **2022**, *34*, 108018. [CrossRef]

44. Cai, S.; Liu, J.; Ding, J.; Fu, Z.; Li, H.; Xiong, Y.; Lian, Z.; Yang, R.; Chen, C. Tumor-Microenvironment-Responsive Cascade Reactions by a Cobalt-Single-Atom Nanozyme for Synergistic Nanocatalytic Chemotherapy. *Angew. Chem. Int. Ed. Engl.* **2022**, *61*, e202204502. [CrossRef]

45. Wu, W.; Wang, Y.; Luo, L.; Wang, M.; Li, Z.; Chen, Y.; Wang, Z.; Chai, J.; Cen, Z.; Shi, Y.; et al. CO$_2$ Hydrogenation over Copper/ZnO Single-Atom Catalysts: Water-Promoted Transient Synthesis of Methanol. *Angew. Chem. Int. Ed. Engl.* **2022**, *61*, e202213024. [CrossRef]

46. Yitao, Z.; Lei, T. Towards catalytic reactions of Cu single-atom catalysts: Recent progress and future perspective. *Chin. Chem. Lett.* **2023**, 108571. [CrossRef]

47. Zhu, Y.; Wang, W.; Cheng, J.; Qu, Y.; Dai, Y.; Liu, M.; Yu, J.; Wang, C.; Wang, H.; Wang, S.; et al. Stimuli-Responsive Manganese Single-Atom Nanozyme for Tumor Therapy via Integrated Cascade Reactions. *Angew. Chem. Int. Ed. Engl.* **2021**, *60*, 9480–9488. [CrossRef] [PubMed]

48. Jiang, Y.; Sung, Y.; Choi, C.; Joo Bang, G.; Hong, S.; Tan, X.; Wu, T.S.; Soo, Y.L.; Xiong, P.; Meng-Jung Li, M.; et al. Single-Atom Molybdenum-N$_3$ Sites for Selective Hydrogenation of CO$_2$ to CO. *Angew. Chem. Int. Ed. Engl.* **2022**, *61*, e202203836. [CrossRef]

49. Xu, B.; Wang, H.; Wang, W.; Gao, L.; Li, S.; Pan, X.; Wang, H.; Yang, H.; Meng, X.; Wu, Q.; et al. A Single-Atom Nanozyme for Wound Disinfection Applications. *Angew. Chem. Int. Ed. Engl.* **2019**, *58*, 4911–4916. [CrossRef] [PubMed]

50. Zhou, S.; Zhao, Y.; Shi, R.; Wang, Y.; Ashok, A.; Heraly, F.; Zhang, T.; Yuan, J. Vacancy-Rich MXene-Immobilized Ni Single Atoms as a High-Performance Electrocatalyst for the Hydrazine Oxidation Reaction. *Adv. Mater.* **2022**, *34*, e2204388. [CrossRef]

51. Quanguo, J.; Yushuai, Q.; Yuqing, L.; Min, H.; Zhimin, A. Strain boosts CO oxidation on Ni single-atom-catalyst supported by defective graphene. *Chin. Chem. Lett.* **2022**, *34*, 107395. [CrossRef]

52. Ai, Y.; Hu, Z.N.; Liang, X.; Sun, H.b.; Xin, H.; Liang, Q. Recent Advances in Nanozymes: From Matters to Bioapplications. *Adv. Funct. Mater.* **2021**, *32*, 107395. [CrossRef]

53. Fan, Y.; Gan, X.; Zhao, H.; Zeng, Z.; You, W.; Quan, X. Multiple application of SAzyme based on carbon nitride nanorod-supported Pt single-atom for H$_2$O$_2$ detection, antibiotic detection and antibacterial therapy. *Chem. Eng. J.* **2022**, *427*, 131572. [CrossRef]

54. Zhao, Y.; Jiang, Y.; Mo, Y.; Zhai, Y.; Liu, J.; Strzelecki, A.C.; Guo, X.; Shan, C. Boosting Electrochemical Catalysis and Nonenzymatic Sensing Toward Glucose by Single-Atom Pt Supported on Cu@CuO Core-Shell Nanowires. *Small* **2023**, *19*, 2207240. [CrossRef] [PubMed]

55. Chen, Y.; Wang, P.; Hao, H.; Hong, J.; Li, H.; Ji, S.; Li, A.; Gao, R.; Dong, J.; Han, X.; et al. Thermal Atomization of Platinum Nanoparticles into Single Atoms: An Effective Strategy for Engineering High-Performance Nanozymes. *J. Am. Chem. Soc.* **2021**, *143*, 18643–18651. [CrossRef]

56. Gu, W.; Wang, H.; Jiao, L.; Wu, Y.; Chen, Y.; Hu, L.; Gong, J.; Du, D.; Zhu, C. Single-Atom Iron Boosts Electrochemiluminescence. *Angew. Chem. Int. Ed. Engl.* **2020**, *59*, 3534–3538. [CrossRef]

57. Qin, J.; Liu, H.; Zou, P.; Zhang, R.; Wang, C.; Xin, H.L. Altering Ligand Fields in Single-Atom Sites through Second-Shell Anion Modulation Boosts the Oxygen Reduction Reaction. *J. Am. Chem. Soc.* **2022**, *144*, 2197–2207. [CrossRef]

58. Wu, N.; Zhong, H.; Zhang, Y.; Wei, X.; Jiao, L.; Wu, Z.; Huang, J.; Wang, H.; Beckman, S.P.; Gu, W.; et al. Atomically dispersed Ru_3 site catalysts for electrochemical sensing of small molecules. *Biosens. Bioelectron.* **2022**, *216*, 114609. [CrossRef] [PubMed]

59. Cheng, N.; Li, J.C.; Liu, D.; Lin, Y.; Du, D. Single-Atom Nanozyme Based on Nanoengineered Fe-N-C Catalyst with Superior Peroxidase-Like Activity for Ultrasensitive Bioassays. *Small* **2019**, *15*, e1901485. [CrossRef]

60. Chen, X.; Wang, Y.; Feng, M.; Deng, D.; Xie, X.; Deng, C.; Khattak, K.N.; Yang, X. Dual-active-site Fe/Cu single-atom nanozymes with multifunctional specific peroxidase-like properties for S^{2-} detection and dye degradation. *Chin. Chem. Lett.* **2022**, *34*, 107969. [CrossRef]

61. Ma, C.B.; Xu, Y.; Wu, L.; Wang, Q.; Zheng, J.J.; Ren, G.; Wang, X.; Gao, X.; Zhou, M.; Wang, M.; et al. Guided Synthesis of a Mo/Zn Dual Single-Atom Nanozyme with Synergistic Effect and Peroxidase-like Activity. *Angew. Chem. Int. Ed. Engl.* **2022**, *61*, e202116170. [CrossRef] [PubMed]

62. Kim, K.; Lee, J.; Park, O.K.; Kim, J.; Kim, J.; Lee, D.; Paidi, V.K.; Jung, E.; Lee, H.S.; Lee, B.; et al. Geometric Tuning of Single-Atom FeN_4 Sites via Edge-Generation Enhances Multi-Enzymatic Properties. *Adv. Mater.* **2023**, *35*, 2207666. [CrossRef] [PubMed]

63. Ji, S.F.; Jiang, B.; Hao, H.G.; Chen, Y.J.; Dong, J.C.; Mao, Y.; Zhang, Z.D.; Gao, R.; Chen, W.X.; Zhang, R.F.; et al. Matching the kinetics of natural enzymes with a single-atom iron nanozyme. *Nat. Catal.* **2021**, *4*, 407–417. [CrossRef]

64. Bian, W.; Shen, X.; Tan, H.; Fan, X.; Liu, Y.; Lin, H.; Li, Y. The triggering of catalysis via structural engineering at atomic level: Direct propane dehydrogenation on Fe-N3P-C. *Chin. Chem. Lett.* **2023**, *34*, 107289. [CrossRef]

65. Jiao, L.; Xu, W.; Zhang, Y.; Wu, Y.; Gu, W.; Ge, X.; Chen, B.; Zhu, C.; Guo, S. Boron-doped Fe-N-C single-atom nanozymes specifically boost peroxidase-like activity. *Nano Today* **2020**, *35*, 100971. [CrossRef]

66. Xu, B.; Li, S.; Zheng, L.; Liu, Y.; Han, A.; Zhang, J.; Huang, Z.; Xie, H.; Fan, K.; Gao, L.; et al. A Bioinspired Five-Coordinated Single-Atom Iron Nanozyme for Tumor Catalytic Therapy. *Adv. Mater.* **2022**, *34*, e2107088. [CrossRef] [PubMed]

67. Wu, F.; Pan, C.; He, C.T.; Han, Y.; Ma, W.; Wei, H.; Ji, W.; Chen, W.; Mao, J.; Yu, P.; et al. Single-Atom $Co-N_4$ Electrocatalyst Enabling Four-Electron Oxygen Reduction with Enhanced Hydrogen Peroxide Tolerance for Selective Sensing. *J. Am. Chem. Soc.* **2020**, *142*, 16861–16867. [CrossRef] [PubMed]

68. Li, J.; Wu, C.; Yuan, C.; Shi, Z.; Zhang, K.; Zou, Z.; Xiong, L.; Chen, J.; Jiang, Y.; Sun, W.; et al. Single-Atom Iron Anchored on 2-D Graphene Carbon to Realize Bridge-Adsorption of O-O as Biomimetic Enzyme for Remarkably Sensitive Electrochemical Detection of H_2O_2. *Anal. Chem.* **2022**, *94*, 14109–14117. [CrossRef]

69. Wei, X.; Song, S.; Song, W.; Xu, W.; Jiao, L.; Luo, X.; Wu, N.; Yan, H.; Wang, X.; Gu, W.; et al. Fe_3C-Assisted Single Atomic Fe Sites for Sensitive Electrochemical Biosensing. *Anal. Chem.* **2021**, *93*, 5334–5342. [CrossRef] [PubMed]

70. Lei, Y.; Butler, D.; Lucking, M.C.; Zhang, F.; Xia, T.; Fujisawa, K.; Nakajima, T.G.; Silva, R.C.; Endo, M.; Terrones, H.; et al. Single-atom doping of MoS_2 with manganese enables ultrasensitive detection of dopamine: Experimental and computational approach. *Sci. Adv.* **2020**, *6*, eabc4250. [CrossRef] [PubMed]

71. Ding, S.; Lyu, Z.; Fang, L.; Li, T.; Zhu, W.; Li, S.; Li, X.; Li, J.C.; Du, D.; Lin, Y. Single-Atomic Site Catalyst with Heme Enzymes-Like Active Sites for Electrochemical Sensing of Hydrogen Peroxide. *Small* **2021**, *17*, e2100664. [CrossRef] [PubMed]

72. Pan, C.; Wu, F.; Mao, J.; Wu, W.; Zhao, G.; Ji, W.; Ma, W.; Yu, P.; Mao, L. Highly Stable and Selective Sensing of Hydrogen Sulfide in Living Mouse Brain with NiN_4 Single-Atom Catalyst-Based Galvanic Redox Potentiometry. *J. Am. Chem. Soc.* **2022**, *144*, 14678–14686. [CrossRef] [PubMed]

73. Gao, X.; Ma, W.; Mao, J.; He, C.T.; Ji, W.; Chen, Z.; Chen, W.; Wu, W.; Yu, P.; Mao, L. A single-atom $Cu-N_2$ catalyst eliminates oxygen interference for electrochemical sensing of hydrogen peroxide in a living animal brain. *Chem. Sci.* **2021**, *12*, 15045–15053. [CrossRef] [PubMed]

74. Liang, Y.; Zhao, P.; Zheng, J.L.; Chen, Y.Y.; Liu, Y.Y.; Zheng, J.; Luo, X.G.; Huo, D.Q.; Hou, C.J. Fe Single-Atom Electrochemical Sensors for H_2O_2 Produced by Living Cells. *Acs Appl. Nano Mater.* **2022**, *5*, 11852–11863. [CrossRef]

75. Li, Z.; Li, Y.; Chen, S.; Zha, Q.; Zhu, M. In-situ monitoring of hydrogen peroxide production at nickel single-atom electrocatalyst. *Chem. Eng. J.* **2023**, *460*, 141657. [CrossRef]

76. Qi, C.; Wang, W.; Dong, Y. Synthesis of Se single atoms on nitrogen-doped carbon as novel electrocatalyst for sensitive nonenzymatic sensing of hydrogen peroxide. *Anal. Bioanal. Chem.* **2023**, *415*, 5391–5401. [CrossRef]

77. Qi, C.; Luo, Y.; Dong, Y. Synergistic effects of Fe-Se dual single-atom sites for boosting electrochemical nonenzymatic H_2O_2 sensing. *Appl. Surf. Sci.* **2023**, *637*, 157900. [CrossRef]

78. Shu, Y.J.; Li, Z.J.; Yang, Y.; Tan, J.W.; Liu, Z.Y.; Shi, Y.H.; Ye, C.X.; Gao, Q.S. Isolated Cobalt Atoms on N-Doped Carbon as Nanozymes for Hydrogen Peroxide and Dopamine Detection. *Acs Appl. Nano Mater.* **2021**, *4*, 7954–7962. [CrossRef]

79. Sun, X.J.; Chen, C.; Xiong, C.; Zhang, C.M.; Zheng, X.S.; Wang, J.; Gao, X.P.; Yu, Z.Q.; Wu, Y.E. Surface modification of MoS_2 nanosheets by single Ni atom for ultrasensitive dopamine detection. *Nano Res.* **2022**, *16*, 917–924. [CrossRef]

80. Xie, X.; Wang, D.P.; Guo, C.; Liu, Y.; Rao, Q.; Lou, F.; Li, Q.; Dong, Y.; Li, Q.; Yang, H.B.; et al. Single-Atom Ruthenium Biomimetic Enzyme for Simultaneous Electrochemical Detection of Dopamine and Uric Acid. *Anal. Chem.* **2021**, *93*, 4916–4923. [CrossRef] [PubMed]

81. Long, B.; Cao, P.; Zhao, Y.; Fu, Q.; Mo, Y.; Zhai, Y.; Liu, J.; Lyu, X.; Li, T.; Guo, X.; et al. Pt_1/Ni_6Co_1 layered double hydroxides/N-doped graphene for electrochemical non-enzymatic glucose sensing by synergistic enhancement of single atoms and doping. *Nano Res.* **2022**, *16*, 318–324. [CrossRef]

82. Long, B.; Zhao, Y.; Cao, P.; Wei, W.; Mo, Y.; Liu, J.; Sun, C.J.; Guo, X.; Shan, C.; Zeng, M.H. Single-Atom Pt Boosting Electrochemical Nonenzymatic Glucose Sensing on $Ni(OH)_2$/N-Doped Graphene. *Anal. Chem.* **2022**, *94*, 1919–1924. [CrossRef] [PubMed]

83. Jiang, J.; Cai, Q.; Deng, M. Construction of Electrochemical Aptamer Sensor Based on Pt-Coordinated Titanium-Based Porphyrin MOF for Thrombin Detection. *Front. Chem.* **2021**, *9*, 812983. [CrossRef]

84. Li, M.; Peng, X.; Liu, X.; Wang, H.; Zhang, S.; Hu, G. Single-atom niobium doped BCN nanotubes for highly sensitive electrochemical detection of nitrobenzene. *RSC Adv.* **2021**, *11*, 28988–28995. [CrossRef] [PubMed]

85. Gu, W.; Wang, X.; Wen, J.; Cao, S.; Jiao, L.; Wu, Y.; Wei, X.; Zheng, L.; Hu, L.; Zhang, L.; et al. Modulating Oxygen Reduction Behaviors on Nickel Single-Atom Catalysts to Probe the Electrochemiluminescence Mechanism at the Atomic Level. *Anal. Chem.* **2021**, *93*, 8663–8670. [CrossRef]

86. Bushira, F.A.; Kitte, S.A.; Xu, C.; Li, H.; Zheng, L.; Wang, P.; Jin, Y. Two-Dimensional-Plasmon-Boosted Iron Single-Atom Electrochemiluminescence for the Ultrasensitive Detection of Dopamine, Hemin, and Mercury. *Anal. Chem.* **2021**, *93*, 9949–9957. [CrossRef] [PubMed]

87. Xia, H.; Zheng, X.; Li, J.; Wang, L.; Xue, Y.; Peng, C.; Han, Y.; Wang, Y.; Guo, S.; Wang, J.; et al. Identifying Luminol Electrochemiluminescence at the Cathode via Single-Atom Catalysts Tuned Oxygen Reduction Reaction. *J. Am. Chem. Soc.* **2022**, *144*, 7741–7749. [CrossRef] [PubMed]

88. Luo, Z.; Xu, W.; Wu, Z.; Jiao, L.; Luo, X.; Xi, M.; Su, R.; Hu, L.; Gu, W.; Zhu, C. Iron Single-Atom Catalyst-Enabled Peroxydisulfate Activation Enhances Cathodic Electrochemiluminescence of Tris(bipyridine)ruthenium(II). *Anal. Chem.* **2023**, *95*, 10762–10768. [CrossRef] [PubMed]

89. Ma, Y.; Zhang, Y.; Gao, J.; Ouyang, H.; He, Y.; Fu, Z. PEGylated Ni Single-Atom Catalysts as Ultrasensitive Electrochemiluminescent Probes with Favorable Aqueous Dispersibility for Assaying Drug-Resistant Pathogens. *Anal. Chem.* **2022**, *94*, 14047–14053. [CrossRef]

90. Tang, Y.; Liu, Y.; Xia, Y.; Zhao, F.; Zeng, B. Simultaneous Detection of Ovarian Cancer-Concerned HE4 and CA125 Markers Based on Cu Single-Atom-Triggered CdS QDs and Eu MOF@Isoluminol ECL. *Anal. Chem.* **2023**, *95*, 4795–4802. [CrossRef] [PubMed]

91. Liu, D.; Wan, X.; Kong, T.; Han, W.; Xiong, Y. Single-atom-based catalysts for photoelectrocatalysis: Challenges and opportunities. *J. Mater. Chem. A* **2022**, *10*, 5878–5888. [CrossRef]

92. Zeng, R.J.; Wang, W.J.; Cai, G.N.; Huang, Z.L.; Tao, J.M.; Tang, D.P.; Zhu, C.Z. Single-atom platinum nanocatalyst-improved catalytic efficiency with enzyme-DNA supermolecular architectures. *Nano Energy* **2020**, *74*, 104931. [CrossRef]

93. Qin, Y.; Wen, J.; Zheng, L.; Yan, H.; Jiao, L.; Wang, X.; Cai, X.; Wu, Y.; Chen, G.; Chen, L.; et al. Single-Atom-Based Heterojunction Coupling with Ion-Exchange Reaction for Sensitive Photoelectrochemical Immunoassay. *Nano Lett.* **2021**, *21*, 1879–1887. [CrossRef] [PubMed]

94. Li, B.; Guo, L.; Chen, M.; Guo, Y.; Ge, L.; Kwok, H.F. Single-atom Pt-anchored $Zn_{0.5}Cd_{0.5}S$ boosted photoelectrochemical immunoassay of prostate-specific antigen. *Biosens. Bioelectron.* **2022**, *202*, 114006. [CrossRef] [PubMed]

95. Zhou, M.; Jiang, Y.; Wang, G.; Wu, W.; Chen, W.; Yu, P.; Lin, Y.; Mao, J.; Mao, L. Single-atom $Ni-N_4$ provides a robust cellular NO sensor. *Nat. Commun.* **2020**, *11*, 3188. [CrossRef]

96. Hou, H.F.; Mao, J.J.; Han, Y.H.; Wu, F.; Zhang, M.N.; Wang, D.S.; Mao, L.Q.; Li, Y.D. Single-atom electrocatalysis: A new approach to in vivo electrochemical biosensing. *Sci. China-Chem.* **2019**, *62*, 1720–1724. [CrossRef]

97. Hu, F.X.; Hu, T.; Chen, S.; Wang, D.; Rao, Q.; Liu, Y.; Dai, F.; Guo, C.; Yang, H.B.; Li, C.M. Single-Atom Cobalt-Based Electrochemical Biomimetic Uric Acid Sensor with Wide Linear Range and Ultralow Detection Limit. *Nanomicro Lett.* **2020**, *13*, 7. [CrossRef] [PubMed]

98. Zhou, W.Y.; Li, S.S.; Xiao, X.Y.; Chen, S.H.; Liu, J.H.; Huang, X.J. Defect- and phase-engineering of Mn-mediated MoS_2 nanosheets for ultrahigh electrochemical sensing of heavy metal ions: Chemical interaction-driven in situ catalytic redox reactions. *Chem. Commun.* **2018**, *54*, 9329–9332. [CrossRef] [PubMed]

99. Yao, L.; Gao, S.; Liu, S.; Bi, Y.; Wang, R.; Qu, H.; Wu, Y.; Mao, Y.; Zheng, L. Single-Atom Enzyme-Functionalized Solution-Gated Graphene Transistor for Real-Time Detection of Mercury Ion. *ACS Appl. Mater. Interfaces* **2020**, *12*, 6268–6275. [CrossRef]

100. Li, P.H.; Yang, M.; Li, Y.X.; Song, Z.Y.; Liu, J.H.; Lin, C.H.; Zeng, J.; Huang, X.J. Ultra-Sensitive and Selective Detection of Arsenic (III) via Electroanalysis over Cobalt Single-Atom Catalysts. *Anal. Chem.* **2020**, *92*, 6128–6135. [CrossRef] [PubMed]

101. Cong, W.; Song, P.; Zhang, Y.; Yang, S.; Liu, W.; Zhang, T.; Zhou, J.; Wang, M.; Liu, X. Supramolecular confinement pyrolysis to carbon-supported Mo nanostructures spanning four scales for hydroquinone determination. *J. Hazard. Mater.* **2022**, *437*, 129327. [CrossRef] [PubMed]

102. Luo, X.; Luo, Z.; Wei, X.; Jiao, L.; Fang, Q.; Wang, H.; Wang, J.; Gu, W.; Hu, L.; Zhu, C. Iridium Single-Atomic Site Catalysts with Superior Oxygen Reduction Reaction Activity for Sensitive Monitoring of Organophosphorus Pesticides. *Anal. Chem.* **2022**, *94*, 1390–1396. [CrossRef] [PubMed]

103. Luo, X.; Yang, M.; Song, W.; Fang, Q.; Wei, X.; Jiao, L.; Xu, W.; Kang, Y.; Wang, H.; Wu, N.; et al. Neutral Zn-Air Battery Assembled with Single-Atom Iridium Catalysts for Sensitive Self-Powered Sensing System. *Adv. Funct. Mater.* **2021**, *31*, 2101193. [CrossRef]

104. Tan, R.; Qin, Y.; Liu, M.; Wang, H.; Su, R.; Xiao, R.; Li, J.; Hu, L.; Gu, W.; Zhu, C. Bifunctional Single-Atom Iron Cocatalysts Enable an Efficient Photoelectrochemical Fuel Cell for Sensitive Biosensing. *Adv. Funct. Mater.* **2023**, 2305673. [CrossRef]